Measurement of internal body time by blood metabolomics

Yoichi Minami[a,1], Takeya Kasukawa[b,1], Yuji Kakazu[c,1], Masayuki Iigo[d], Masahiro Sugimoto[c,e], Satsuki Ikeda[c], Akira Yasui[f], Gijsbertus T. J. van der Horst[g], Tomoyoshi Soga[c,2], and Hiroki R. Ueda[a,b,2]

[a]Laboratory for Systems Biology, and [b]Functional Genomics Unit, RIKEN Center for Developmental Biology, 2-2-3 Minatojima-minamimachi, Chuo-ku, Kobe, Hyogo 650-0047, Japan; [c]Institute for Advanced Biosciences, Keio University, 246-2 Mizukami Kakuganji, Tsuruoka-shi, Yamagata 997-0052, Japan; [d]Department of Applied Biochemistry, Utsunomiya University, 350 Mine-machi, Utsunomiya, Tochigi 321-8505, Japan; [e]Department of Bioinformatics, Mitsubishi Space Software Co., Ltd., 5-4-36, Tsukaguchi-Honmachi, Amagasaki, Hyogo 661-0001, Japan; [f]Department of Molecular Genetics, Institute of Development, Aging and Cancer, Tohoku University, Seiryo-machi 4-1, Aobaku, Sendai, Miyagi 980-8575, Japan; and [g]MGC, Department of Genetics, Erasmus University Medical Center, P.O. Box 2040, 3000 CA Rotterdam, The Netherlands

Edited by Joseph S. Takahashi, Northwestern University, Evanston, IL, and approved April 21, 2009 (received for review January 22, 2009)

Detection of internal body time (BT) via a few-time-point assay has been a longstanding challenge in medicine, because BT information can be exploited to maximize potency and minimize toxicity during drug administration and thus will enable highly optimized medication. To address this challenge, we previously developed the concept, ''molecular-timetable method,'' which was originally inspired by Linné's flower clock. In Linné's flower clock, one can estimate the time of the day by watching the opening and closing pattern of various flowers. Similarly, in the molecular-timetable method, one can measure the BT of the day by profiling the up and down patterns of substances in the molecular timetable. To make this method clinically feasible, we now performed blood metabolome analysis and here report the successful quantification of hundreds of clock-controlled metabolites in mouse plasma. Based on circadian blood metabolomics, we can detect individual BT under various conditions, demonstrating its robustness against genetic background, sex, age, and feeding differences. The power of this method is also demonstrated by the sensitive and accurate detection of circadian rhythm disorder in jet-lagged mice. These results suggest the potential for metabolomics-based detection of BT (''metabolite-timetable method''), which will lead to the realization of chronotherapy and personalized medicine.

chronotherapy | circadian | metabolome | jet-lag | LC-MS

In the 18th century, the Swedish botanist Karl von Linné designed a "flower clock" comprising a series of plant species arranged according to the respective time of the day their flowers open or close. Watching this flower clock, one can estimate the time of the day by noting the pattern of flower opening and closing. Since Linné's early times, it has been a well known fact that plants have an internal clock and thereby can open or close their flowers at a precise time of the day. Similarly, animals possess an internal molecular mechanism, a "circadian clock," which underlies endogenous, self-sustained oscillations with a period of ≈24 h manifest in diverse physiological and metabolic processes (1). In mammals, several clock genes, including *Clock*, *Bmal1*, *Per1*, *Per2*, *Cry1*, *Cry2*, *RevErbA*, *Rora*, *Csnk1e*, *Csnk1d*, and *Fbxl3*, regulate, at least in part, gene expression in central and/or peripheral clock tissues (2–4). Reflecting the temporal changes in gene expression in central and peripheral clock tissues (5–8), the potency and/or toxicity of administered drugs depend on the individual's present body time (BT) (9–13). It has been suggested that administrating a drug at a specific BT improves the outcome of pharmacotherapy by maximizing its potency and minimizing its toxicity (14). In contrast, administrating a drug at an inappropriate BT can result in severe side effects (15). Despite the importance of such BT-dependent therapy (also known as "chronotherapy") (9–13), its application to clinical practice has been obstructed by a lack of clinically feasible methods for measuring BT.

To overcome this problem, we previously developed the concept of a "molecular-timetable method (16)," which was originally inspired by Linné's flower clock. In Linné's flower clock, one can estimate the time of the day by watching the opening and closing pattern of various flowers. Similarly, in molecular-timetable method, one can measure the BT of the day by profiling the up and down pattern of substances in the molecular timetable. This concept was proven using the expression profile of clock-controlled genes in a target organ (16). However, estimates of BT from the expression profile of oscillating substances within a target organ (in this case, the liver) are hard to apply directly to clinical situations. To make the molecular-timetable method more clinically relevant, we decided to determine BT from blood samples, which are more available in clinical practice.

In the blood of mammals, several small chemical substances such as metabolites and hormones have been reported to exhibit circadian oscillations. For example, the concentration of the steroid hormone, corticosterone, is rhythmically controlled by circadian clock with a peak in the evening (17), and an amine-derived hormone, melatonin, show circadian rhythm with a peak in the early morning in mice (18). In humans, several peptide hormone levels show daily variations; growth hormone increases during sleep (19), leptin increases during the evening (20), and prolactin increases at night (21). Concentrations of amino acids, including tryptophan, tyrosine, phenylalanine (22), methionine (23), cysteine, glutathione (24), and homocysteine (25), also exhibit daily variations in human blood plasma. Despite these findings, comprehensive profiling of circadian dynamics of chemical substances in mammalian blood has not yet been reported, and until now a comprehensive molecular timetable of such chemical substances has not been constructed.

Metabolomics technology aims to comprehensively identify and/or quantify the dynamic chemical substances present in biological samples. It is gaining interest in the fields of drug discovery, disease diagnostics, and treatment (26–28). The present metabolomics technology was developed rapidly by coupling advanced separation technology with highly sensitive and selective mass spectrometry–gas chromatography mass spectrometry (GC/MS) (29–31), liquid chromatography mass spectrometry (LC-MS) (32–34), and capillary electrophoresis mass spectrometry (CE-MS) (35, 36). To construct the molecular timetable from clinically available samples, we have performed blood metabolome analysis in this study. Using the LC-MS technique, we quantified hundreds of

Author contributions: Y.M., T.K., T.S., and H.R.U. designed research; Y.M., T.K., Y.K., M.I., and S.I. performed research; M.S., A.Y., and G.T.J.v.d.H. contributed new reagents/analytic tools; T.K. analyzed data; and Y.M., T.K., T.S., and H.R.U. wrote the paper.

The authors declare no conflict of interest.

This article is a PNAS Direct Submission.

Freely available online through the PNAS open access option.

[1]Y.M., T.K., and Y.K. contributed equally to this work.

[2]To whom correspondence may be addressed. E-mail: soga@sfc.keio.ac.jp or uedah-tky@umin.ac.jp.

This article contains supporting information online at www.pnas.org/cgi/content/full/0900617106/DCSupplemental.

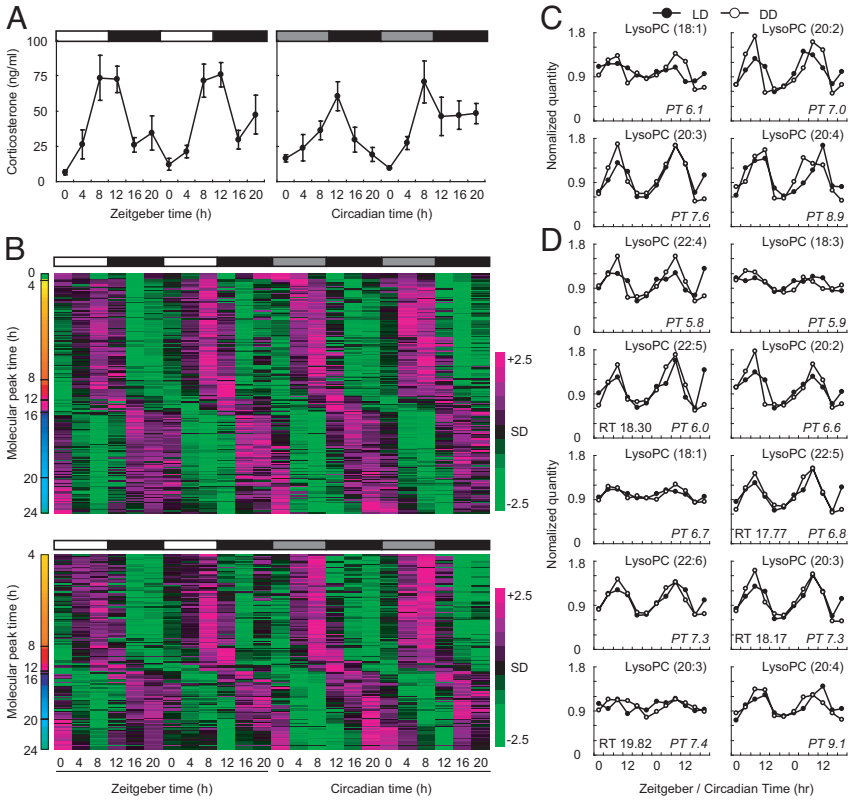

Fig. 1. Circadian patterns of metabolites in mouse plasma. (*A*) Circadian changes in corticosterone levels in the plasma of CBA/N mice under LD (*Left*) and DD, *Center*) conditions. All values are mean ± SEM. The white bars above the graph indicate day, gray bars indicate subjective day, and black bars indicate night/subjective night. ZT0 is the time of light on, and CT0 is the time the light used to be turned on. (*B*) Circadian oscillatory metabolites in the plasma of CBA/N mice [negative ions (up); positive ions (down)]. On the heat maps, magenta tiles indicate a high quantity of substances and green tiles indicate a low quantity in plasma. Metabolites are sorted according to their molecular peak time (molecular peak times are indicated as colors). (*C* and *D*) Identified oscillatory peaks measured by negative ion mode (*C*) and positive ion mode (*D*). Mean value was set to 1.0.

clock-controlled metabolites in mouse plasma and successfully constructed a molecular timetable of blood metabolites. This metabolite timetable allowed us to measure individual BT under various conditions and was robust enough to be used in mice with different genetic backgrounds, sex, age, and feeding conditions. It was also sensitive and accurate enough to detect circadian rhythm disorders in jet-lagged mice. Our preliminary results suggest that other metabolomics techniques such as CE-MS can also be applied to the molecular-timetable method, demonstrated by the quantification of hundreds of clock-controlled metabolites, the identification of substantial portion of these metabolites, and successful measurement of BT from independent blood samples. Thus, metabolomics-based measurement of BT will contribute to the potential areas of chronotherapy and personalized medication regimens.

Results

Construction of the Metabolite Timetable from Blood Plasma by LC-MS. Samples of blood plasma were taken from young male CBA/N mice every 4 hours over 2 days during light–dark (LD) or constant darkness (DD) conditions. Plasma corticosterone was used as a quality control because it exhibits a clear circadian oscillation when quantified by radio immunoassay (Fig. 1*A*). Small chemical substances in the plasma were quantified by LC-MS analysis to construct the metabolite timetable. LC-MS analysis detected 695 negative ion and 938 positive ion peaks in the plasma. Of these, 176 negative and 142 positive ion peaks exhibited significant circadian oscillations in LD and DD conditions [Fig. 1*B*; false discovery rate (FDR) <0.01; see also *Materials and Methods*]; these peaks accounted for the ≈19.5% of the peaks detected in mouse plasma. These substances served as "time-indicating metabolites," because they oscillate considerably even under constant environmental conditions (DD). For instance, at zeitgeber time 0 (ZT0; the beginning of day) or circadian time 0 (CT0; the beginning of a subjective day), concentrations of dawn-indicating metabolites, which peak at approximately ZT0 or CT0 (Fig. 1*B*, green color bars in the molecular peak time), are high, whereas those of dusk-indicating metabolites, which peak at approximately ZT12 or CT12 (Fig. 1*B*, red color bars in the molecular peak time), are low. Conversely, at ZT12 or CT12, concentrations of dawn-indicating metabolites are low, whereas those of dusk-indicating metabolites are high; this suggests that time-indicating metabolites can represent BT (BT), the endogenous state of circadian clock. In fact, the oscillations of these time-indicating metabolites are directly or indirectly controlled by circadian clock, because the disruption of functional molecular clock in *Cry1*−/−, *Cry2*−/− mice (37) results in the alteration of circadian oscillations of these metabolites (Fig. S1). We used these LC-MS data to construct the molecular timetable of time-indicating metabolites (a "metabolite timetable") in mouse plasma (Table S1 online). We also note that, among these time-indicating metabolites (i.e., oscillatory peaks detected by LC-MS), 14 oscillatory peaks were identified as various types of lysophosphatidylcholines with different unsaturated fatty acids (Fig. 1 *C* and *D*).

Measurement of BT from Independent Samples. To verify whether the metabolite timetable was a good indicator of BT, we attempted to estimate the BT from the metabolite profiles of independently sampled mice. We collected fresh blood plasma from individual young male CBA/N mice every 4 h over 24 h under both LD or DD conditions because of the possibility that sampling time and/or light conditions would affect the accuracy of BT estimation. LC-MS analysis was performed to profile the time-indicating metabolites in the plasma samples (Fig. 2 *A* and *B*). After measured profile of the time-indicating metabolites was normalized by using the metabolite timetable, we filtered out outliers, fitted the normalized profile to cosine curve, and calculated the significance of its fitness (see also *Materials and Methods*). This metabolite-timetable method could successfully detect significant circadian rhythmicity in all metabolite profiles of these samples ($P < 0.01$, Fig. 2 *A* and *B*). The estimated BT closely matched with the environmental time when sampled (ZT under LD condition or CT under LD condition) with estima-

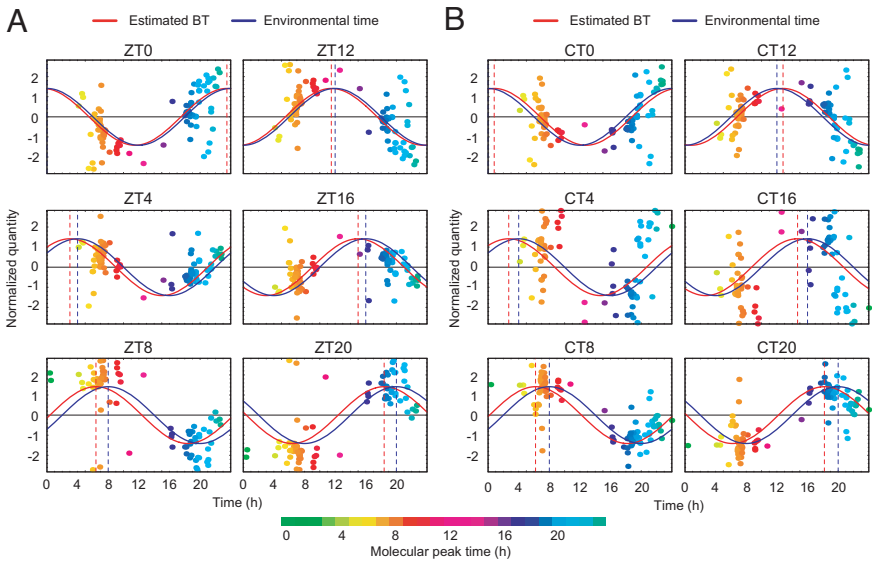

Fig. 2. BT estimation. BT measurements of mice kept under LD (*A*) and DD (*B*) conditions. Colors of the dots indicate the molecular peak times of each substance (Table S1). Peak time of the red cosine curves indicates estimated BT and peak time of the blue indicates the time the sample was taken (''environmental time''). The greater the degree of overlap of the red and blue curves, the greater the accuracy of the measurement. The dashed vertical lines show the BT (red) or environmental time (ZT/CT, blue). See Table S2 for statistics.

tion errors of 1.0 ± 0.49 h for LD and 1.3 ± 0.45 h for DD (mean ± SD, Table S2). Estimation error was here defined as time difference between estimated BT and sampling time (environmental time). These results suggest that BT can be accurately determined from the metabolite profiles of independently sampled mice.

Differences in Genetic Backgrounds. In clinical situations, methods for BT detection must apply to populations with heterogeneous genetic backgrounds. To demonstrate the suitability of the metabolite-timetable method for individuals with different genetic backgrounds, we applied the method to other inbred mouse strain with genetic backgrounds that differed from the original CBA/N strain. We chose C57BL/6, because C57BL/6 and CBA/N are genetically remote from each other and classified into 2 completely different clusters among 55 mice strains according to SNP-based study (38). We collected the blood plasma samples from individual young male C57BL/6 mice every 4 h over 24 h under LD and DD conditions and quantified the time-indicating metabolites in the plasma by LC-MS (Fig. 3 *A* and *B*). The metabolite-timetable method detected significant circadian rhythmicity ($P < 0.01$) in all metabolite profiles both under LD (Fig. 3*A*) and DD conditions (Fig. 3*B*) even if we used the metabolite timetable constructed from CBA/N mice. The estimated BT closely matched with the environmental time with the estimation errors of 1.6 ± 0.36 h for LD and 1.7 ± 0.24 h for DD (mean ± SD, Table S2). These results suggest that BT can be accurately determined from the metabolite profiles of mice with heterogeneous genetic backgrounds.

Differences in Age and Sex. We constructed the metabolite timetable from young male mice only, so it was possible that age and sex factors might affect the accuracy of the metabolite-timetable method. To determine the influence of age and sex, we also applied the metabolite-timetable method to aged male and young female mice of the same strain. Blood plasma from individual aged male or young female CBA/N mice was sampled at 2 time points, ZT0 (the beginning of the day, i.e., time of light on) and ZT12 (the end of the day, i.e., time of the light off) under LD condition. These time points were considered as 2 "noisiest" time points, because light conditions were dramatically changed at these points. Time-indicating metabolites in the plasma were quantified by LC-MS (Fig. 4*A*) and significant circadian rhythmicity ($P < 0.01$) was detected in all metabolite profiles of both the aged male mice and

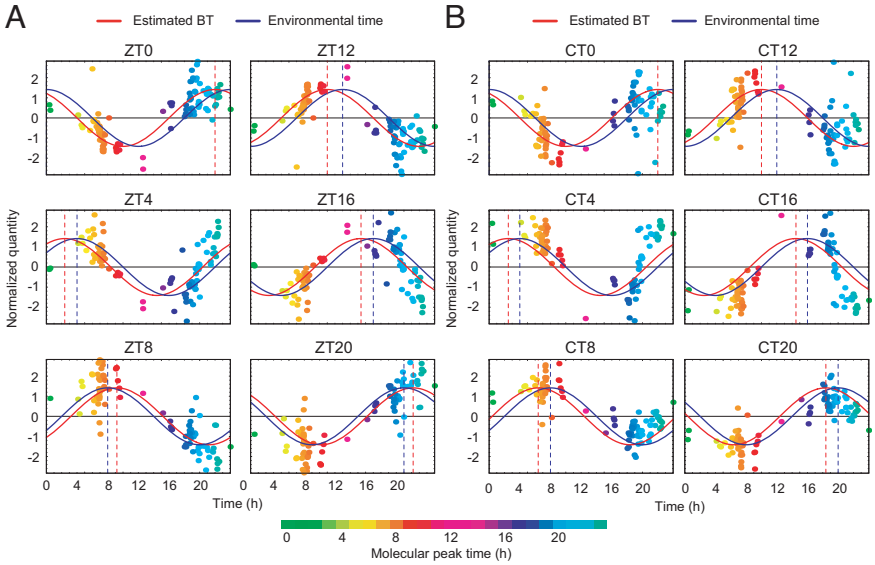

Fig. 3. Genetic background. BT measurement using C57BL/6 mice plasma collected under LD (*A*) and DD (*B*) conditions. Colors of the dots indicate the molecular peak times of each substance (Table S1). Peak time of the red cosine curves indicate estimated BT and peak time of the blue indicate the environmental time. The dashed vertical lines show the BT (red) or environmental time (ZT/CT, blue). See Table S2 for statistics.

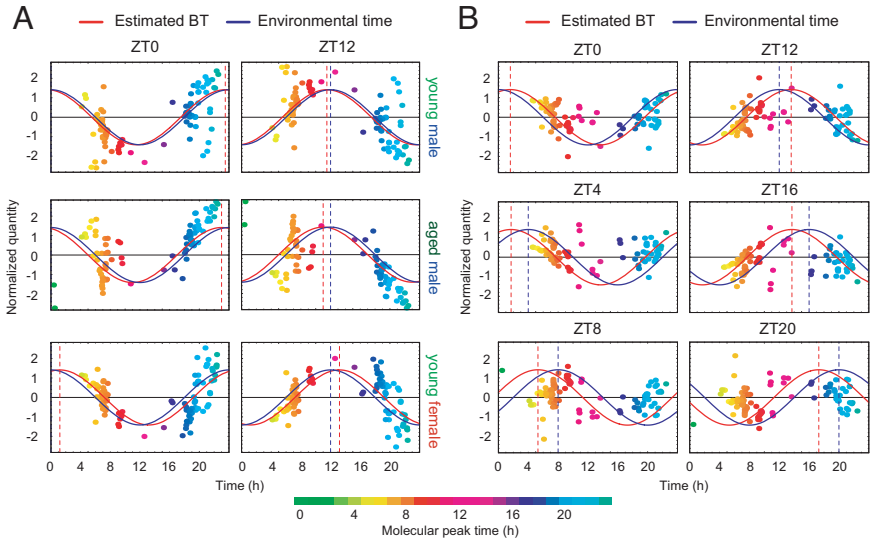

Fig. 4. Age, sex differences and feeding condition. (*A*) BT measurement of young male (*Top*), aged male (*Middle*), and young female mice plasma (*Bottom*) harvested at ZT0 (*Left*) and ZT12 (*Right*). (*B*) BT measurement of young male mice kept under food-deprivation conditions. Colors of the dots indicate the molecular peak times of each substance (Table S1). Peak time of the red cosine curves indicates estimated BT, and peak time of the blue indicates the environmental time. The dashed vertical lines show the BT (red) or environmental time (ZT, blue). Results for young male mice (*A*) are replotted from Fig. 2*A* for comparison. See also Table S2 for statistics.

the young female CBA/N mice (Fig. 4*A*). The estimated BT from individual mice sampled at ZT0 and ZT12 were BT23.0 and BT11.0 in aged male mice and BT1.2 and BT13.2 in young female mice (Table S2). These results demonstrate that BT can be accurately determined from the metabolite profiles of mice of different age and sex.

Differences in Feeding Conditions. The circadian rhythmicity of food intake is well known (39); therefore, feeding conditions may severely affect the accuracy of the metabolite-timetable method. To validate the use of the metabolite timetable in individuals with different feeding conditions, we applied the metabolite-timetable method to CBA/N mice deprived of food (food deprivation). This feeding condition differed greatly from the original feeding condition where CBA/N mice were allowed ad lib feeding. We collected the blood plasma from individual young, male, food-deprived CBA/N mice every 4 hours over 24 h under LD condition. LC-MS analysis was performed to quantify the plasma metabolites (Fig. 4*B*). The metabolite-timetable method detected significant circadian rhythmicity ($P < 0.03$) in all metabolite profiles. The estimated BT matched with the environmental time with the estimation errors of 2.2 ± 0.50 h (mean ± SD, Table S2). These results suggest that BT can be determined from the metabolite profiles of mice even under severe feeding conditions.

Detection of Jet Lag. The final stage of the study was to evaluate the use of the metabolite-timetable in the diagnosis of circadian rhythm disorders. Jet lag is a common disorder of circadian rhythm, in which there is a difference between the internal BT and environmental time. To mimic jet lag, we kept the mice for 2 weeks under normal LD conditions and then rapidly advanced the lighting schedule by 8 h (40). Plasma samples were analyzed at 2 time points (ZT0 and ZT12 of the original LD cycle, termed as "Time 1" and "Time 2") on 3 separate days: on day 1 (before entrainment to the new cycle), day 5 (during entrainment), and day 14 (after entrainment) (Fig. 5 *A* and *B*). On day 1, the estimated BTs were 23.8 h (Time 1) and 11.8 h (Time 2), suggesting that the internal BTs still follow the original LD cycle. By day 14, estimated BTs were 8.8 h (Time 1) and 20.8 h (Time 2), suggesting that the internal BTs had shifted by ≈8 h from the original LD cycle and had therefore become entrained completely to the advanced cycle. Notably, on day 5, estimated BTs were 3.5 h (Time 1) and 15.5 h (Time 2), a shift

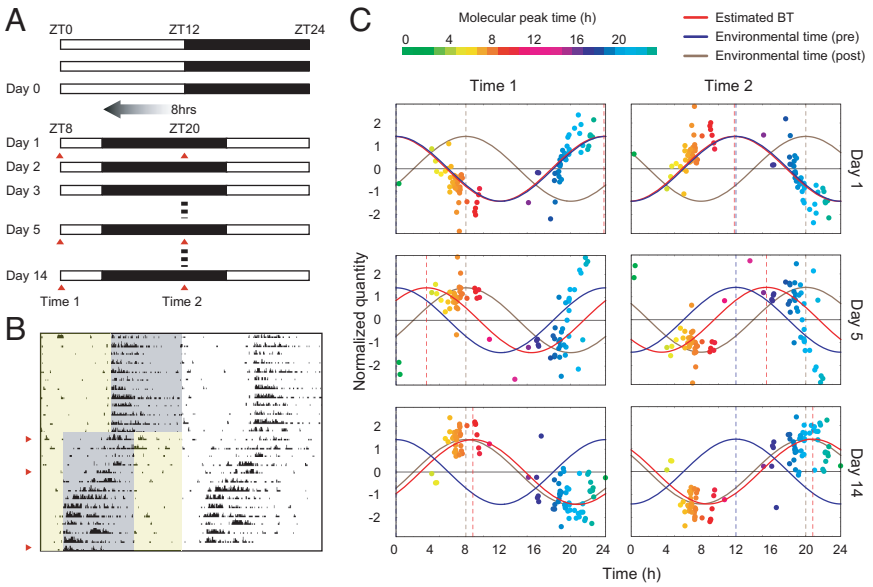

Fig. 5. Detection of jet lag. (*A*) Schematic view of lighting conditions. White bars indicate light on, and black bars indicate light off. On day 1, the light was turned off 8 h earlier. Samples were collected at 2 time points on days 1, 5, and 14 after the LD shift (red triangles). (*B*) The actogram of a single mouse, showing that it was experiencing "jet lag" induced by the LD shift. Yellow shading indicates periods of light on, and gray shading indicates periods of light off. The red triangles indicate days 1 (*Top*), 5 (*Middle*), and 14 (*Bottom*). (*C*) BT measurement from mouse plasma collected before (day 1, *Top*), during (day 5, *Middle*), and after entrainment to the new LD cycle (day 14, *Lower*). Colors of the dots indicate the molecular peak time of each substance (Table S1). The red cosine curve is the estimation, the blue curve is the environmental time (pre LD condition shift), and the brown cosine curve is the environmental time (post shift). See also Table S2 for statistics.

of 3.5 h from the original LD cycle, indicating incomplete entrainment to the advanced cycle, i.e., jet lag (Fig. 5*C* and Table S2). These results suggest that the metabolite-timetable method can accurately detect circadian rhythm disorders. Another set of BT estimation data for jet-lagged mice supports this conclusion (Fig. S2 and Table S2).

General Applicability of the Metabolite-Timetable Method: CE-MS-Based Method. As described above, the metabolite-timetable method based on LC-MS analysis can accurately measure the individual's BT and sensitively diagnose circadian rhythm disorders such as jet lag. The method depends entirely on the oscillations of numerous chemical substances and time-indicating metabolites; therefore, it can be applied to other metabolomics technologies such as CE-MS analysis. With CE-MS analysis, it is possible to separate charged compounds. So this is a complementary technology to LC-MS analysis (35). To demonstrate the general applicability of the metabolite-timetable method to other metabolomics technology, blood plasma was sampled and pooled from young male CBA/N mice every 4 hours under LD or DD conditions over 2 days. Small positively charged chemical substances in these samples were quantified by CE-MS, which detected 953 peaks. Of these peaks, 153 exhibited significant circadian oscillations under LD and DD conditions (Fig. S3*A*). We used these CE-MS data to construct the metabolite timetable in mouse plasma (Table S3). Notably, 28 peaks (18.3% of the total) were identified as known metabolites (Fig. S3*B*).

To confirm whether the CE-MS-based metabolite timetable was a good indicator of an individual's BT, we estimated BT from the metabolite profiles of independently sampled mice. Fresh plasma from young male CBA/N mice was collected every 4 hours over 24 h both under LD and DD conditions. CE-MS analysis was performed to profile the time-indicating metabolites (Fig. S3 *C* and *D*). The CE-MS-based metabolite-timetable method detected significant circadian rhythmicity in all metabolite profiles of these samples ($P < 0.01$, Fig. S3 *C* and *D*). The estimated BT was close to the environmental time with estimation errors of 0.6 ± 0.29 h for LD and 0.6 ± 0.54 h for DD (mean ± SD, Table S4). These results suggest the metabolite-timetable method is generally applicable to other metabolomics technologies such as CE-MS. See Fig. S3 *E–H* and *SI Text* for the result at a more stringent criterion (FDR < 0.01).

Discussion

We identified 14 and 28 oscillatory peaks in mouse blood as known metabolites in LC-MS and CE-MS analysis, respectively. For example, a different type of lysophsophatidylcolines exhibit significant circadian oscillations in LC-MS analysis (Fig. 1 *C* and *D*). The genes for key enzymes synthesizing lysophosphatidylcoline are *Lcat* (lecitine:cholesterol acyltransferase), *Lipc* (hepatic lipase), and *Lipg* (endothelial lipase). Among these genes, *Lcat* and *Lipc* are mainly expressed in liver. We found that *Lipc* mRNA are rhythmically expressed in the mouse liver with the peak time around peak time (PT) 5 (8), which slightly proceeds with the peak time of identified oscillatory lysophosphatidylcolines (PT5.8–9.1). In CE-MS analysis, many amino acids exhibit significant circadian rhythmicity. For example, glutamine (Gln), threonine (Thr), proline (Pro), valine (Val), phenylalanine (Phe), methionine (Met), isoleucine (Ile), leucine (Leu), and tryptophan (Trp) peak at around midnight (≈PT18), whereas glycine (Gly) peaks in the evening (PT12.1) (Fig. S4). In the urea cycle, metabolites such as ornithine (PT18.6), citrulline (PT19.9), and 4-guanidino-butyrate (PT20.1) exhibit significant circadian rhythmicity (FDR <0.1). Arginine (Arg), which plays an important role in the urea cycle, also exhibits suggestive circadian rhythmicity (FDR = 0.215; PT0.6) in our CE-MS data. It is also noteworthy that the final product—Urea—is reported to vary over 24 h in the blood of certain species such as rabbits (41) and rats (42). Interestingly, Reddy et al. (43) showed that 3 key enzymes involved in the urea cycle, carbamoyl-phosphate synthetase 1 (CPS1), argininosuccinate synthetase 1 (ASS1), and arginase 1 (ARG1), show circadian rhythms in the liver, the center of the urea cycle and urea formation (43). In the creatine pathway and neighboring glycine and threonine metabolism, metabolites such as guanidoacetate (PT6.2), Creatine (PT14.7), creatinine (PT18.7), sarcosine (PT18.0), and dimethylglycine (PT16.5) exhibit significant circadian rhythmicity (FDR <0.1). Arginine (PT0.6) first converts to guanidoacetate. Guanidoacetatete (CT6.2) then converts to creatine. Creatine (PT14.7) finally converts to creatinine (PT18.7) or sarcosine (PT18.0), which is also converted from dimethylglycine (PT16.5). The differences in the peak times of these metabolites may reflect successive processing throughout the day in the creatine pathway and neighboring glycine and threonine metabolism (Fig. S4).

Our results suggest that metabolite-timetable method can detect circadian rhythm disorders in vivo. In a normal situation, patients live under the zeitgeber (e.g., light). Notably, our method successfully diagnoses the jet-lag state under LD conditions (Fig. 5 and Fig. S2), and this strongly suggests that endogenous abnormal clock state can be diagnosed by our method, even if there is external time information such as light. Circadian rhythm disorders are caused by environmental factors (such as jet lag) and/or inherited factors (as in familial advanced sleep-phase syndrome). Brown et al. (44, 45) reported detecting circadian rhythm disorders by characterizing the feature of molecular circadian clocks in the isolated cells. They collected skin samples from human subjects, cultured the cells, and transfected clock-controlled reporter into the cells. The features of the molecular circadian clock in the isolated cells correlated with the chronotypes (i.e., the feature of organismal circadian clock) of the subjects, suggesting that the method should also allow detection of inherited circadian rhythm disorders. Our method can detect both inherited and acquired circadian rhythm disorders but cannot distinguish between them, whereas Brown et al.'s (44, 45) method can detect inherited but not acquired disorders. These 2 methods are therefore complementary for detecting circadian rhythm disorders.

Although our results suggest the metabolite-timetable method can successfully estimate BT, keeping MS and hiring a specialized operator in each hospital seems difficult. Establishing a special center for "detecting BT" performing MS analysis is 1 possibility to solve this. Another possibility is detecting time-indicating metabolites in a specific way (e.g., making an ELISA kit for detecting BT using a specific antibody for target time-indicating metabolites). To achieve the latter possibility, the assignment of oscillatory peaks to known metabolites is important, and we already identified 14 (LC-MS) and 28 (CE-MS) oscillatory peaks as known metabolites (Figs. 1 and S3). We also examined the effect of peak numbers on BT estimation. Fig. S5 shows the accuracy of the BT estimation using the different number of oscillatory metabolites. If we set the statistical error rate $P < 0.05$ and estimation error between environmental and estimated time <2 h, the minimum number of time-indicating metabolites was ≈20. In addition, the effect of feeding is an important issue, especially in humans, because humans eat different amounts of food at entirely different times. Further analysis on food intake conditions would be a great help for applying this method in clinical situations.

In this study, we showed that a metabolite-timetable method based on LC–MS analysis is able to estimate individuals' BTs with a high degree of accuracy throughout the time of the day, under different lighting conditions (LD and DD), and in individuals with different genetic backgrounds (CBA/N and C57BL/6 mice) (Figs. 2 and 3). We also found that the LC–MS-derived metabolite timetable is robust despite differences in age, sex, and feeding (Fig. 4); in addition, it is a sensitive and accurate detector of disordered circadian rhythm in jet-lagged mice. Our preliminary results suggest that the metabolite-timetable method can be also applied to other metabolomics techniques such as CE–MS; it allowed quantification of hundreds of clock-controlled metabolites, of which many could

be identified, enabling successful measurement of BT from independent blood samples. The next step is to construct a metabolite timetable for human blood plasma, which will help measurement of BTs for humans and diagnosis of circadian rhythm disorders and facilitate the development of chronotherapy and tailored medication regimens.

Materials and Methods

BT Measurement. Metabolomics-based measurement of BT is performed as described for expression-based measurement of BT (16), except that 2 samples are used for an estimation of BT. In the metabolite-timetable method, we used 2 samples with 12-h sampling time interval (e.g., ZT0 and ZT12 are used for 1 measurement of BT) to calibrate measurement-to-measurement experimental fluctuations of detection sensitivity, which usually differs among metabolites. We define the area in a certain sample as A_{si} and the mean areas of 2 samples (of 12-h time interval) as M_{si} for metabolite i. We also define the mean, standard deviation, and peak time of metabolite i in the timetable as M_{ti}, S_{ti}, and p_{ti}, respectively. For estimation of BT, we did not use outlying metabolites that do not satisfy the condition ($|(M_{ti} - M_{si})/S_{ti}| < 2\sqrt{2}$). By changing b to 0, 0.1, . . . , 23.9, we searched for b with a maximum Pearson's correlation between $\{\sqrt{2}\cos(2\pi(P_{ti} - b)/24)\}$ and $\{(A_{si} - M_{si})/S_{ti}\}$, and we predicted b as BT of the target sample. To estimate the P value of the prediction, we applied a permutation test to the maximum correlations.

Ethics. All experiments were performed with the permission of Kobe Animal Experiment Supervisory Panel (permission IDs are AH15-10 and AH18-01).

Supporting Information. More Materials and Methods information is available in *SI Text*.

ACKNOWLEDGMENTS. We thank Sachie Satoh and Yuki Ueno for technical support. We also thank Shigenobu Shibata, Masamitsu Iino, Kenichiro Uno, Rikuhiro Yamada, Hideki Ukai, Guojun Sheng, Yasushi Isojima, and Sato Honma for helpful discussions and Erik Kuld for proofreading of the manuscript. The Laboratory for Animal Resources and Genetic Engineering in the Center for Developmental Biology is noted for assistance with mouse work. This work is partly supported by New Energy Developing Organization (NEDO) (H.R.U.), a grant on Priority Aeas ''Ensuring Chemical Hazard'' and ''Biomarker Discovery for Drug Development'' from the Health and Labor Sciences Research Grants (T.S.), and a grant ''Functional Genomics on Fundamental Brain Functions'' from Utsunomiya University (M.I.).

1. Dunlap JC, Loros JJ, DeCoursey PJ, eds (2004) *Chronobiology: Biological Timekeeping* (Sinauer, Sunderland, MS).
2. Reppert SM, Weaver DR (2002) Coordination of circadian timing in mammals. *Nature* 418:935–941.
3. Ueda HR (2007) Systems biology of mammalian circadian clocks. *Cold Spring Harb Symp Quant Biol* 72:365–380.
4. Takahashi JS, Hong HK, Ko CH, McDearmon EL (2008) The genetics of mammalian circadian order and disorder: Implications for physiology and disease. *Nat Rev Genet* 9:764–775.
5. Akhtar RA, et al. (2002) Circadian cycling of the mouse liver transcriptome, as revealed by cdna microarray, is driven by the suprachiasmatic nucleus. *Curr Biol* 12:540–550.
6. Panda S, et al. (2002) Coordinated transcription of key pathways in the mouse by the circadian clock. *Cell* 109:307–320.
7. Storch KF, et al. (2002) Extensive and divergent circadian gene expression in liver and heart. *Nature* 417:78–83.
8. Ueda HR, et al. (2002) A transcription factor response element for gene expression during circadian night. *Nature* 418:534–539.
9. Halberg F (1969) Chronobiology. *Annu Rev Physiol* 31:675–725.
10. Labrecque G, Belanger PM (1991) Biological rhythms in the absorption, distribution, metabolism and excretion of drugs. *Pharmacol Ther* 52:95–107.
11. Lemmer B, Scheidel B, Behne S (1991) Chronopharmacokinetics and chronopharmacodynamics of cardiovascular active drugs. Propranolol, organic nitrates, nifedipine. *Ann NY Acad Sci* 618:166–181.
12. Reinberg A, Halberg F (1971) Circadian chronopharmacology. *Annu Rev Pharmacol* 11:455–492.
13. Reinberg A, Smolensky M, Levi F (1983) Aspects of clinical chronopharmacology. *Cephalalgia 3 Suppl* 1:69–78.
14. Levi F, Zidani R, Misset JL (1997) Randomised multicentre trial of chronotherapy with oxaliplatin, fluorouracil, and folinic acid in metastatic colorectal cancer. International organization for cancer chronotherapy. *Lancet* 350:681–686.
15. Ohdo S, Koyanagi S, Suyama H, Higuchi S, Aramaki H (2001) Changing the dosing schedule minimizes the disruptive effects of interferon on clock function. *Nat Med* 7:356–360.
16. Ueda HR, et al. (2004) Molecular-timetable methods for detection of body time and rhythm disorders from single-time-point genome-wide expression profiles. *Proc Natl Acad Sci USA* 101:11227–11232.
17. Kennaway DJ, Owens JA, Voultsios A, Varcoe TJ (2006) Functional central rhythmicity and light entrainment, but not liver and muscle rhythmicity, are clock independent. *Am J Physiol* 291:R1172–R1180.
18. Kennaway DJ, Voultsios A, Varcoe TJ, Moyer RW (2002) Melatonin in mice: Rhythms, response to light, adrenergic stimulation, and metabolism. *Am J Physiol* 282:R358–R365.
19. Takahashi Y, Kipnis DM, Daughaday WH (1968) Growth hormone secretion during sleep. *J Clin Invest* 47:2079–2090.
20. Schoeller DA, Cella LK, Sinha MK, Caro JF (1997) Entrainment of the diurnal rhythm of plasma leptin to meal timing. *J Clin Invest* 100:1882–1887.
21. Kok P, et al. (2006) Increased circadian prolactin release is blunted after body weight loss in obese premenopausal women. *Am J Physiol* 290:E218–E224.
22. Breum L, Rasmussen MH, Hilsted J, Fernstrom JD (2003) Twenty-four-hour plasma tryptophan concentrations and ratios are below normal in obese subjects and are not normalized by substantial weight reduction. *Am J Clin Nutr* 77:1112–1118.
23. Forslund AH, et al. (2000) Inverse relationship between protein intake and plasma free amino acids in healthy men at physical exercise. *Am J Physiol Endocrinol Metab* 278:E857–E867.
24. Blanco RA, et al. (2007) Diurnal variation in glutathione and cysteine redox states in human plasma. *Am J Clin Nutr* 86:1016–1023.
25. Bonsch D, et al. (2007) Daily variations of homocysteine concentration may influence methylation of DNA in normal healthy individuals. *Chronobiol Int* 24:315–326.
26. Fernie AR, Trethewey RN, Krotzky AJ, Willmitzer L (2004) Metabolite profiling: From diagnostics to systems biology. *Nat Rev Mol Cell Biol* 5:763–769.
27. Kell DB, et al. (2005) Metabolic footprinting and systems biology: The medium is the message. *Nat Rev Microbiol* 3:557–565.
28. Villas-Boas SG, Mas S, Akesson M, Smedsgaard J, Nielsen J (2005) Mass spectrometry in metabolome analysis. *Mass Spectrom Rev* 24:613–646.
29. Fiehn O, et al. (2000) Metabolite profiling for plant functional genomics. *Nat Biotechnol* 18:1157–1161.
30. Fiehn O, Kopka J, Trethewey RN, Willmitzer L (2000) Identification of uncommon plant metabolites based on calculation of elemental compositions using gas chromatography and quadrupole mass spectrometry. *Anal Chem* 72:3573–3580.
31. Schauer N, et al. (2006) Comprehensive metabolic profiling and phenotyping of interspecific introgression lines for tomato improvement. *Nat Biotechnol* 24:447–454.
32. Plumb R, et al. (2003) Metabonomic analysis of mouse urine by liquid-chromatography-time of flight mass spectrometry (lc-tofms): Detection of strain, diurnal and gender differences. *Analyst* 128:819–823.
33. Wilson ID, et al. (2005) High resolution ''Ultra performance'' Liquid chromatography coupled to oa-tof mass spectrometry as a tool for differential metabolic pathway profiling in functional genomic studies. *J Proteome Res* 4:591–598.
34. Tolstikov VV, Lommen A, Nakanishi K, Tanaka N, Fiehn O (2003) Monolithic silica-based capillary reversed-phase liquid chromatography/electrospray mass spectrometry for plant metabolomics. *Anal Chem* 75:6737–6740.
35. Soga T, et al. (2006) Differential metabolomics reveals ophthalmic acid as an oxidative stress biomarker indicating hepatic glutathione consumption. *J Biol Chem* 281:16768–16776.
36. Soga T, et al. (2003) Quantitative metabolome analysis using capillary electrophoresis mass spectrometry. *J Proteome Res* 2:488–494.
37. van der Horst GT, et al. (1999) Mammalian cry1 and cry2 are essential for maintenance of circadian rhythms. *Nature* 398:627–630.
38. Tsang S, et al. (2005) A comprehensive snp-based genetic analysis of inbred mouse strains. *Mamm Genome* 16:476–480.
39. Froy O, Miskin R (2007) The interrelations among feeding, circadian rhythms and ageing. *Prog Neurobiol* 82:142–150.
40. Moriya T, et al. (1998) Potentiating action of mkc-242, a selective 5-ht1a receptor agonist, on the photic entrainment of the circadian activity rhythm in hamsters. *Br J Pharmacol* 125:1281–1287.
41. Piccione G, Caola G, Refinetti R (2007) Daily rhythms of liver-function indicators in rabbits. *J Physiol Sci* 57:101–105.
42. Kato H, Mizutani-Funahashi M, Shiosaka S, Nakagawa H (1978) Circadian rhythms of urea formation and argininosuccinate synthetase activity in rat liver. *J Nutr* 108:1071–1077.
43. Reddy AB, et al. (2006) Circadian orchestration of the hepatic proteome. *Curr Biol* 16:1107–1115.
44. Brown SA, et al. (2005) The period length of fibroblast circadian gene expression varies widely among human individuals. *PLoS Biol* 3:e338.
45. Brown SA, et al. (2008) Molecular insights into human daily behavior. *Proc Natl Acad Sci USA* 105:1602–1607.

Supporting Information

Minami et al. 10.1073/pnas.0900617106

SI Text

CE–MS-Based Metabolite-Timetable Method with More Stringent Criterion. As described in the main text, CE-MS analysis detected 953 peaks from blood plasma samples. Among these peaks, 44 peaks exhibit significant circadian oscillations under more stringent oscillation criterion (FDR <0.01, Fig. S3*E*). Ten peaks, corresponding to 22.7% of these peaks of circadian oscillations, were identified as known metabolites (Fig. S3*F*). Based on these detected and/or identified time-indicating metabolites by CE-MS analysis, we can construct the metabolite timetable in mice blood plasma (see Table S3).

To verify the possibility that this metabolite timetable well represent BT of individuals, we attempted to estimate the BT from the metabolite profiles of independently sampled mice. We assessed the metabolite profiles of fresh blood plasma from individual young male CBA/N mice every 4 h over 24 h both under LD or DD conditions (Fig. S3 *G* and *H*). As expected, we can significantly detect circadian rhythmicity in all metabolite profiles of these samples ($P < 0.01$, Fig. S3 *G* and *H*). The estimated BT closely matched with the sampling time with the estimation errors, 1.5 ± 0.76 h for LD condition and 1.4 ± 0.90 h for DD condition (mean ± SD). These results suggest that the CE–MS -based method, with the time-indicating metabolites selected by the same stringent criterion (FDR < 0.01) as the LC-MS-based method, can accurately detect the internal BT of independently sampled individuals (Table S4).

Possible Mechanisms to Generate Circadian Oscillations of Metabolites. In this study, we found many oscillatory metabolites in mice blood by LC-MS (176 peaks for negative ions and 142 peaks for positive ions) and by CE-MS (153 peaks for positive ions). There are possible mechanisms to generate circadian oscillations of metabolites. The first possible mechanism is the regulation of the physiological input (e.g., food intake) and output (e.g., behavioral activity) by circadian clock. Through these regulations, the metabolites are rhythmically supplied, and/or rhythmically consumed in the body. The second possibility is the direct regulation of the key regulatory enzymes of the target metabolic pathways by circadian clock. For example, circadian clock system can regulate transcription of key enzymes via clock-controlled elements including E-box, DBP-binding element (D-box) and Rev-erb/ROR binding element (RRE) (1, 2). Posttranscriptional regulation of these enzymes may be included in this possibility. The third possibility would be more indirect/additional effects on the metabolism by the circadian clock. Circadian clock controls many physiological phenomena like hormonal secretions. For example, secreted hormones can also regulate endogenous metabolites state rhythmically.

The Possible Tissue Sources of the Circadian Oscillations of Blood Metabolites and the Possible Mechanisms to Generate the Biased Distribution of Their Phase. Strictly speaking, there is no single internal body time because different tissues have different internal time with phase differences. Therefore, it is worthwhile to discuss about the possible tissue sources to generate the circadian rhythmicity of metabolites in blood. As we discussed in the main text, we found in LC-MS analysis that lysophsophatidylcoline exhibited significant circadian oscillations in mice blood, which might be generated by circadian oscillations of a key enzyme synthesizing lysophosphatidylcoline, *Lipc* (hepatic lipase) in the liver (3). We note that *Lipc* mRNA are rhythmically expressed in the mouse liver with the peak time around PT5 (3), which slightly proceeds with the peak time of identified oscillatory lysophosphatidylcolines (PT 5.8-PT 9.1). In CE-MS analysis, we found that metabolites in urea cycle exhibit circadian oscillations. Urea generation is one of the main functions in liver. We note that mRNA of *Asl*, which represents the gene for key enzyme involved in urea generation, is rhythmically expressed in the mouse liver with the peak time around PT18 (3). Reddy et al. (4) reported that protein levels of CPS1, ASS1, and ARG1 show circadian rhythmicity. ASS1 converts citrulline to argininosuccinate and the CPS acts as the rate-limiting step in ureagenesis by converting ammonia to carbamoyl phosphate. According to their data, ASS1 and CPS peaked during circadian night when nocturnal feeding and digestion would present amino acids to the hepatocytes, whereas ARG1, the final stage before urea production, peaked later in circadian day, when digestion would have been complete (4). According to these results, the contribution of the liver seems important for generating circadian oscillations of the blood metabolites. We also note that observed distribution of peak time of blood metabolites converges into 2 phases (i.e., around midday and around midnight). This might be because specific metabolic pathways are controlled by circadian clocks. Actually, as we discussed in the above, the identified metabolites in LC-MS and CE-MS are involved in a few specific pathways such as lysophosphatidylcoline pathway peaking around midday (Fig. 1), and urea cycles and glycine-threonine metabolism peaking around midnight (Fig. S4B). Further assignment of the oscillatory peaks to known metabolites should contribute to unveil the mechanism to generate circadian oscillations of blood metabolites and the biased distribution of their phase.

Why We Focused on Cosine-Wave-Like Metabolites. In this study, we focused on cosine-wave-like metabolites by fitting time-course data of blood metabolite concentrations to cosine wave (*SI Materials and Methods*). This is because the estimation of peak time of circadian metabolites of cosine-wave form is not affected by the time points in the construction of molecular timetable (if these are of 4-h time intervals). We also note that we calculated a continuous peak time of each oscillatory metabolite from the wave-form of its time-course data. Theoretically speaking, the calculated (continuous) peak time of metabolites doe not depend on the time points in the construction of molecular timetable when we focus on the cosine-wave-like metabolite as we did in this study. Therefore, even if the test samples are collected at any time points in-between these time points, it doesn't affect the estimation of body time.

Because we focused only on cosine-wave-like metabolites, we might miss circadian metabolites of noncosine wave form in this study. To find such noncosine-wave-like metabolites, another type of statistical filter will be helpful. For example, the ANOVA test with periodicity test like autocorrelation is 1 possibility. In addition, a more narrow time window (i.e., 1 or 2 h) and/or more long-term (e.g., 3 or 4 days) sampling might be also helpful.

SI Materials and Method

Animals. CBA/N mice were purchased from Japan SLC. Young male or female mice were 5–6 weeks old, and aged male mice were "retired breeders", aged ≈6 months. Male C57BL/6 mice (5–6 weeks old) were purchased from Charles River. All mice were kept under light–dark (LD; light 12 h, dark 12 h) conditions over 2 weeks with food pellets (CRF-1, Charles River) and water given ad libitum. *Cry1*−/− and *Cry2*−/− mice were originally

generated by A.Y. and G.T.J.v.d.H, and the founder population was transported from Tohoku University to RIKEN CDB, where they were maintained and reproduced.

Sampling Schedule. Sampling of mouse plasma was performed under both LD and DD conditions. For DD sampling, the housing condition was changed to constant darkness on the day that sampling began. Sampling was started at ZT0/CT0. Trunk body blood was collected in tubes containing Novoheparin (Mochida Pharm) every 4 h for 2 days (12 samples in total).

Fasted mice were food deprived by removing food pellets from their cages at the light-off point 1 day before sampling began. They were deprived of food until their trunk blood was collected. Sampling began at ZT4 (4 h after light on) and ended at ZT0 the next day (6 time points). Immediately before they were killed, they were weighed to determine how much weight they had lost. To extract the plasma, blood was centrifuged twice at 1,000 × *g* for 5 min at 4 °C. Supernatants were withdrawn and stored at −80 °C in a deep-freezer until RIA or metabolome analysis was performed.

Jet-Lag Experiment. Young male CBA/N mice were maintained under LD cycles (light 12 h, dark 12 h) for 2 weeks. Then the lighting schedule was shifted by 8 h (day 1). The mice were killed, and trunk blood was collected on days 1, 5, and 14. Their behavior was monitored by an infrared monitoring system (NS-AS01, Neuroscience) and data were visualized with *Clock-Lab* software (Actimetrix).

Corticosterone RIA. [1,2,6,7-^{3}H(N)]-Corticosterone (NET-399, 2.6 TBq/mmol) and the rabbit anticorticosterone serum (FKA-420) were obtained from PerkinElmer Japan and Cosmo Bio, respectively. After the addition of 200 μl of the assay buffer (Gel-PBS; 20 mM phosphate buffer containing 0.1% gelatin and 140 mM NaCl), plasma samples (5 μl) were extracted with diethylether (1 ml for 2 times). The organic phase was separated from the aqueous phase and evaporated with a vacuum evaporator. The residue was dissolved in 250 microliters of Gel-PBS and 50-microliter aliquots were subjected to RIA. A standard curve (6.25–800 pg/tube) was constructed by using serial 2-fold dilutions of authentic corticosterone (Sigma) dissolved in Gel-PBS. For the initiation of RIA, anticorticosterone serum (1:10,000 dilution with PBS containing 50 mM EDTA, 100 μl) and [1,2,6,7-^{3}H(N)]-corticosterone (≈10,000 dpm in Gel-PBS, 100 μl) were added to test tubes containing Gel-PBS and the standard or samples (200 μl in total). After incubation for 24 h at 4 °C, dextran-coated charcoal solution (200 μL; Norit SX-3, 0.5 g/L, Wako Pure Chemicals, and 0.05 g/L dextran T-70, Amersham Pharmacia, in 20 mM phosphate buffer containing 140 mM NaCl, 50 mM EDTA, and 0.1% sodium azide, pH 7.5; EDTA-PBS) and incubated for 15 min at 4 °C until centrifugation (2,000 × *g*) for 15 min at 4 °C. The supernatant was decanted into a scintillation vial (Pony Vial, PerkinElmer Japan) containing 2 mL of scintillant (Clearsol-1, Nakalai Tesque). The tube was capped and mixed, and then the radioactivity was counted in a liquid scintillation counter (Aloka). Parallelism of inhibition curves was proved between serial 2-fold dilution of corticosterone standard and the plasma extract (data not shown). Intra- and interassay coefficients of variation were 7.3% (n = 10) and 8.4% (n = 16) at the 500 pg/tube level, respectively. The minimum detectable level defined as 2 standard deviations from the buffer control was <62.5 pg/tube. Cross-reactivities of the antiserum according to the manufacturer were as follows: deoxycorticosterone, 4.80%; 11-dehydrocorticosterone, 4.70%; progesterone 5.40%; cortisol, 2.20%; 4-androstenedione, 1.20%; cortisone, 0.23%; 17-hydroxy-11-deoxycorticosterone, 0.19%; 17alpha-hydroxyprogesterone, 0.30%; testosterone, 0.35%; aldosterone, pregnenolone, 17alpha-hydroxy-prognenolone, dehydroepiandrosterone, and estradiol-17beta, <0.01%.

LC–MS Samples. After acetonitrile (225 μL) was added, plasma samples were shaken and centrifuged. Supernatants were placed in new tubes and dried. Acetonitrile (25 μL) was added to the samples before analyzing the metabolites.

LC-MS Conditions. The LC system used was an Agilent 1100 series HPLC (Agilent Technologies). The ZORBAX SB-C18 RRHT (φ2.1 50 mm, 1.8 μm) was purchased from Agilent Technologies, and columns were kept at 60 °C. The mobile phase consisted of 0.1% acetic acid/water as A and methanol as B. The gradient went from 40% B in 0 min, 99% in 20 min, 99% in 30 min, 40% in 30.01 min, and then kept at 40% B until 40 min. The flow rate was 0.2 mL/min, and the injection volume was 1 μL. MS data were acquired on a Qstar XL mass spectrometry (Applied Biosystems). Samples were analyzed by both positive and negative ion electrospray mass spectrometry. The MS conditions for positive ions (positive, TOF scan mode) were as follows: spray voltage, 5.5 kilovolts; scan range m/z 250–700; curtain gas, 20 arbitrary units (nitrogen); gas 1, 50 arbitrary unit; gas 2, 50 arbitrary units (500 °C). Declustering potential 1/2 was 50 volts/15 volts. The MS conditions for negative ions (negative ion mode, TOF scan) was almost of the same as positive ion conditions, but the spray voltage was −4.5 kilovolts and declustering potential 1/2 was −50 volts/−15 volts.

LC-MS/MS Conditions. We performed LC-MS/MS for associating oscillatory peaks to known chemicals as described in the previous report (5) with little modified. The LC system used was an Agilent 1100 series HPLC (Agilent Technologies) and the mobile phase consisted of 0.1% acetic acid/water as A and methanol as B. MS data were acquired on a Qstar XL mass spectrometry (Applied Biosystems).

CE–MS Samples. To select oscillatory substances, pooled mouse plasma (4–10 mice per time point) was used; individual mouse plasma was used for BT measurement. Plasma samples (100 μL) were plunged into 1.8 mL of methanol containing 55 μM each methionine sulfone and 2-Morpholinoethanesulfonic acid (Mes) and mixed well. Then 800 μL of deionized water and 2 mL of chloroform were added, and the solution was centrifuged at 2,500 × *g* for 5 min at 4 °C. The 800-μL upper aqueous layer was centrifugally filtered through a Millipore 5-kDa cutoff filter to remove proteins. The filtrate was lyophilized and dissolved in 50 μL of Milli-Q water containing reference compounds (200 μM each of 3-aminopyrrolidine and trimesate) before CE-TOFMS analysis.

Metabolite Standards for CE-MS. All chemical standards were obtained from common commercial sources and dissolved in Milli-Q (Millipore) water, 0.1 N HCl or 0.1 N NaOH to obtain 10 or 100 mM stock solutions. Working standard mixtures were prepared by diluting stock solutions with Milli-Q water immediately before injection into the CE-TOFMS. The chemicals used were of analytical or reagent grade.

Instrumentation for CE–MS. All CE-TOFMS experiments were performed using an Agilent CE capillary electrophoresis system (Agilent Technologies), an Agilent G3250AA LC/MSD TOF system (Agilent Technologies), an Agilent1100 series binary HPLC pump, and the G1603A Agilent CE–MS adapter and G1607A Agilent CE-ESI-MS sprayer kit. For system control and data acquisition, we used the G2201AA Agilent ChemStation software for CE and the Analyst QS for Agilent TOFMS software. CE-MS/MS analyses for compound identification were

performed on a Q-Star XL Hybrid LC–MS/MS System (Applied Biosystems) connected to an Agilent CE instrument.

CE-TOFMS Conditions for Cationic Metabolite Analysis. Separations were carried out in a fused silica capillary (50-μm inner diameter × 100-cm total length) filled with 1 M formic acid as the electrolyte (6). ×48 ≈3 nL of the sample solution was injected at 50 mbar for 3 s and 30 kilovolts of voltage applied. The capillary temperature was maintained at 20 °C, and the sample tray was cooled below 5 °C. Methanol water (50% vol/vol) containing 0.5 μM reserpine was delivered as the sheath liquid at 10 μL/min. ESI-TOFMS was operated in the positive ion mode, and the capillary voltage was set at 4 kilovolts. A flow rate of heated dry nitrogen gas (heater temperature 300 °C) was maintained at 10 psig. In TOFMS, the fragmentor, skimmer and Oct RFV voltages were set at 120, 50, and 200 volts, respectively. Automatic recalibration of each acquired spectrum was performed using reference masses of reference standards. The methanol adduct ion ($[2MeOH + H_2O + H]^+$, m/z 65.0597) and reserpine ($[M^+H]^+$, m/z 609.2806) provided the lock mass for exact mass measurements. Exact mass data were acquired at a rate of 10 spectra/s over a 50–1,000 m/z range.

Associating Peaks of LC–MS Data. The LC–MS dataset comprises 3 series of samples. The first series included the following sample sets for making a metabolite timetable: pooled CBA/N young male plasma collected under LD ($n = 5$ per time point), DD ($n =$ 4–6 per time point) and pooled *Cry1*−/−, *Cry2*−/− plasma ($n =$ 2 per time point). The second series included the following sample sets for BT measurement: individual CBA/N plasma collected under LD and DD; individual C57BL/6 plasma collected under LD and DD; and aged male and young female CBA/N mice under LD and young male CBA/N undergoing jet lag. The third series included CBA/N plasma collected during food deprivation. Samples in a single series were measured within 2 days: 1 day for positive ions and the other for negative ions. There are longer intervals between the measuring dates of 3 series (≈3 months between the first and the second series and ≈1 year between the first and the third series).

For the intraseries peak association, we used Marker View software (Applied Biosystems). We set the detection range of the migration time from 3 to 28 min. For the interseries peak association, we first corrected retention time (RT) according to the reported method (7), then we associated the peaks in 2 series with the smallest values of:

(difference of m/z between 2 series/X)^2 + (difference of RT between 2 series/Y)^2 in peaks with (difference of m/z) $< X$ and (difference of RT) $< Y$ in both series. Parameters X and Y were determined by the following procedure: (*i*) the values of X and Y were changed (e.g., $X = 0.01, 0.02, .., 0.15$ and $Y = 0.1, 0.2, .., 1.5$) and peaks were associated. (*ii*) Pearson's correlations of the associated peak area were calculated, and P values were estimated. (*iii*) We then chose the parameter sets with the smallest P values. In this procedure, the best parameter sets were $X = 0.09$, $Y = 0.5$ (positive ions), and $X = 0.13$, $Y = 0.4$ (negative ions) for the first and the second series and $X = 0.11$, $Y = 0.9$ (positive ions) and $X = 0.15$, $Y = 1.3$ (negative ions) for the first and the third series.

Associating Peaks of CE−MS Data. We associated peaks of CE-MS data with the KEIO MasterHANDs software (8), in which automated algorithm and manual curation are used.

Normalization of Peak Areas. For the LC-MS data, 1 (centroid) sample was chosen from 24 LD/DD pooled samples (this centroid sample had the largest mean of Pearson's correlation with the other 23 samples). Centroid samples were independently chosen for positive and negative ion data. Then, for each sample, linear regression to the function $Y = X + a$ was performed on the areas of the target (X) and centroid sample (Y), and normalized areas of the target samples according to the fitted linear function by subtracting the fitted value a from the target areas. For the CE-MS data, each area was normalized by dividing it by the area of the internal control (methionine sulfone) spiked into each sample.

Making the Metabolite Timetable. First, we chose substances that were detected at 10 or more time points in both LD and DD conditions. Next, for each chosen metabolite, area values in LD and DD were scaled to have the same mean values in LD and DD. For the scaled areas, we searched for the maximum Pearson's correlation of a cosine curve over a 24-h period and its phase with a Fourier transformation-based method (9). We then estimated P values and FDRs by permutation tests. Substances that have FDR <0.01 for LC-MS data and both FDR <0.01 and FDR <0.1 for CE-MS data were selected as significantly oscillating metabolites. We focused on cosine-wave-like metabolites, because the estimation of peak time of circadian metabolites of cosine-wave form is not affected by the time points in the construction of metabolite timetable.

Metabolic Map. Identified circadian oscillatory metabolites were put on the known metabolic map, and the metabolic map was generated through the use of Ingenuity Pathways Analysis (ver. 7.0, Ingenuity Systems).

Estimating a Lower Bound of Peak Counts in a Reliable Timetable. To estimate a lower limitation of the number of peaks in a timetable, we performed BT estimation algorithm with shrunk timetables. For choosing n peaks in a timetable, all positive and negative ion peaks were sorted by P value (FDR) of their circadian oscillation and by correlations to cosine curves within the same P values, and the best n peaks were retrieved. By changing the number of peaks (n) within a range between 3 and 200, BTs of LD and DD individual samples were estimated with the shrunk timetables, and mean estimation errors and P values were calculated.

1. Ueda HR, et al. (2005) System-level identification of transcriptional circuits underlying mammalian circadian clocks. *Nat Genet* 37:187–192.
2. Kumaki Y, et al. (2008) Analysis and synthesis of high-amplitude cis-elements in the mammalian circadian clock. *Proc Natl Acad Sci USA* 105:14946–14951.
3. Ueda HR, et al. (2002) A transcription factor response element for gene expression during circadian night. *Nature* 418:534–539.
4. Reddy AB, et al. (2006) Circadian orchestration of the hepatic proteome. *Curr Biol* 16:1107–1115.
5. Taguchi R, et al. (2005) Focused lipidomics by tandem mass spectrometry. *J Chromatogr B Analyt Technol Biomed Life Sci* 823:26–36.
6. Soga T, Heiger DN (2000) Amino acid analysis by capillary electrophoresis electrospray ionization mass spectrometry. *Anal Chem* 72:1236–1241.
7. Soga T, et al. (2006) Differential metabolomics reveals ophthalmic acid as an oxidative stress biomarker indicating hepatic glutathione consumption. *J Biol Chem* 281:16768–16776.
8. Baran R, et al. (2006) Mathdamp: A package for differential analysis of metabolite profiles. *BMC Bioinformatics* 7:530.
9. Chatfield C (1996) *The Analysis of Time Series: An Introduction* (Chapman and Hall/CRC, London).

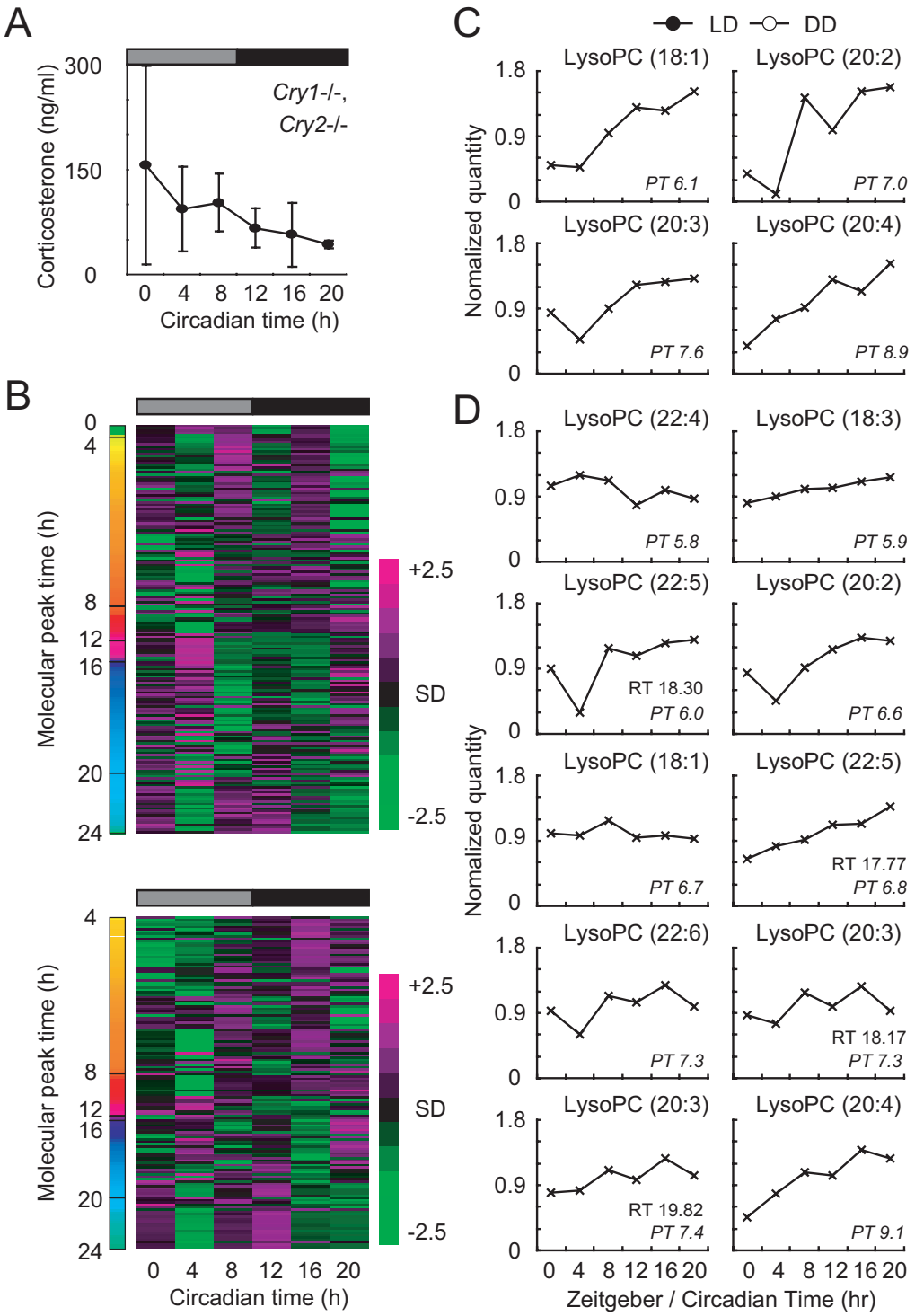

Fig. S1. Circadian patterns of metabolites in *Cry1-/-*, *Cry2-/-* mice plasma. (*A*) Nonrhythmic pattern of corticosterone in *Cry1-/-*, *Cry2-/-* ($n = 2$) mice under DD conditions. (*B*) Time indicating metabolites loose their rhythmicity in *Cry1-/-*, *Cry2-/-* mice plasma. Negative ion (*Upper*) and positive ion (*Lower*) are presented as heat maps where magenta tiles indicate a high quantity of substances and green tiles indicate a low quantity in plasma. Color bars beside the heat maps indicate molecular peak time of each metabolite (Fig. 1). (*C* and *D*) Identified oscillatory peaks of *Cry1-/-*, *Cry2-/-* mice measured by negative ion mode (*C*) and positive ion mode (*D*). Mean value was set to 1.0.

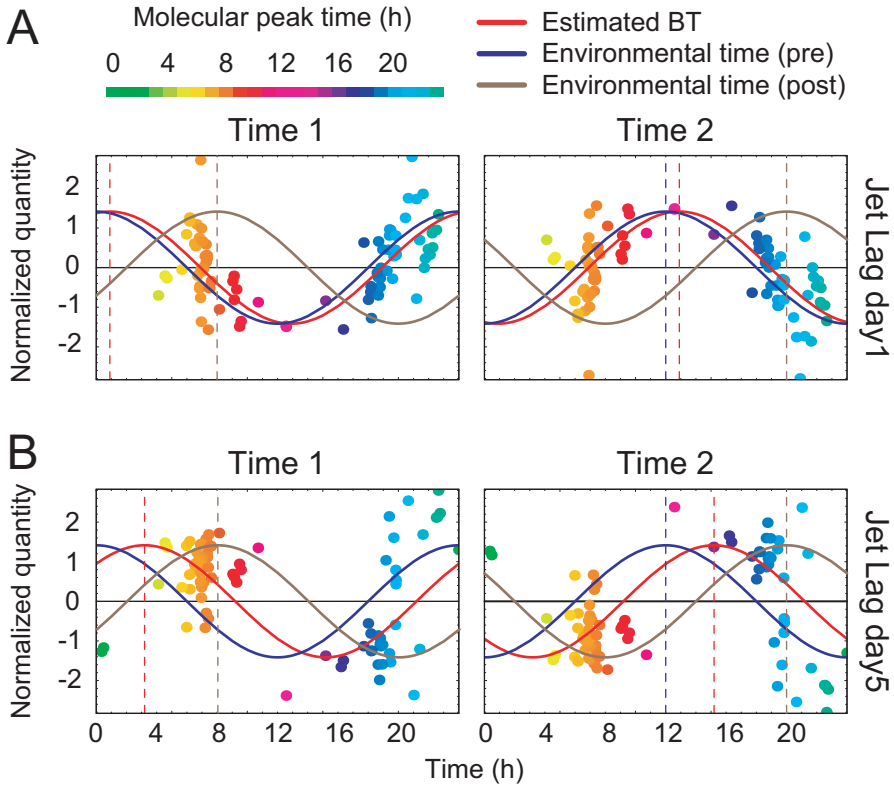

Fig. S2. Results of BT estimations. (*A* and *B*) BT measurement from mouse plasma collected before (day 1, *A*) and during entrainment to the new LD cycle (day 5, *B*). Colors of the dots indicate the molecular peak time of each substance (Table S1). The red cosine curve is the estimation, the blue curve is the environmental time (pre-LD condition shift), and the brown cosine curve is the environmental time (postshift). See also Table S2 for statistics.

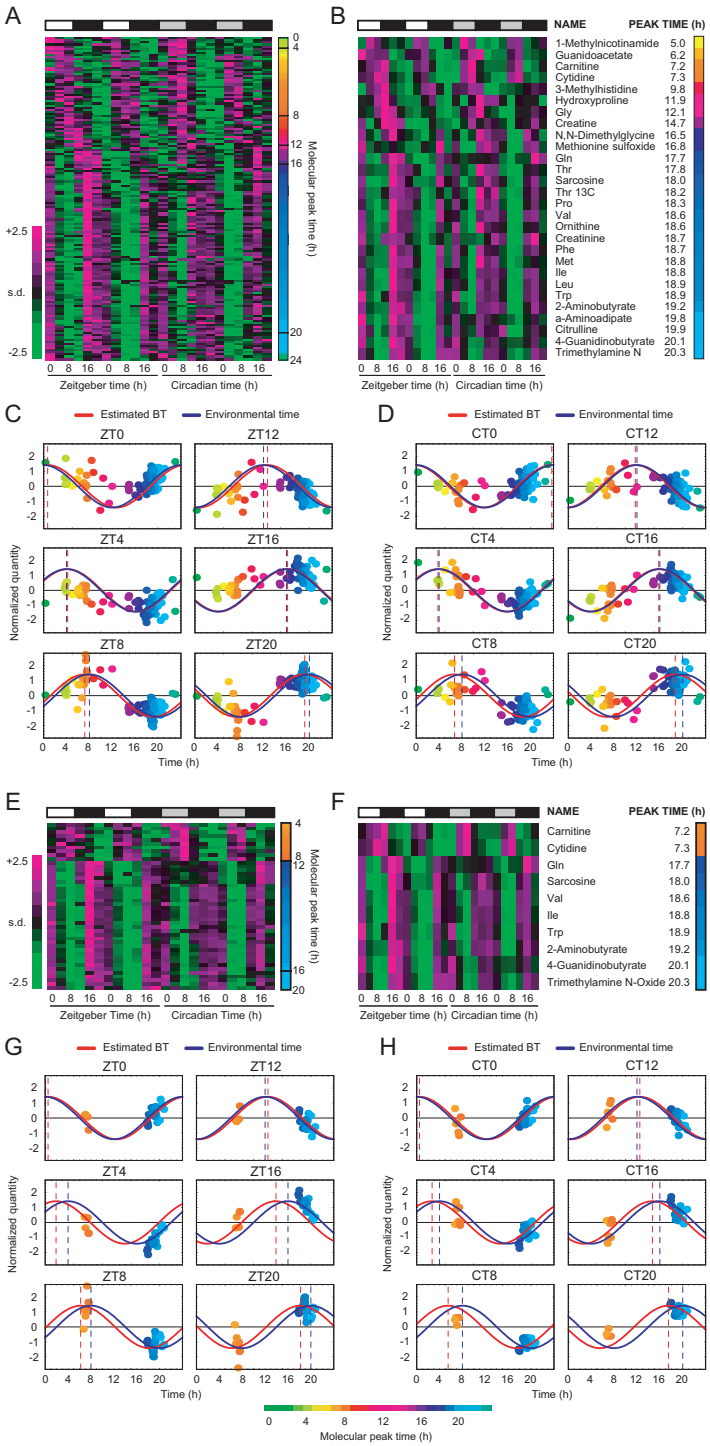

Fig. S3. The metabolite-timetable method based on CE-MS analysis. (*A* and *B*) Circadian oscillatory metabolites in mouse plasma (positive ion, FDR <0.1) (*A*) and identified oscillatory substances (*B*). (*C* and *D*) BT measurements of mice kept under LD (*C*) and DD (*D*) conditions. (*E* and *F*) Circadian oscillatory metabolites in mouse plasma (positive ion, FDR <0.01) (*E*) and identified oscillatory substances (*F*). On the heat maps, magenta tiles indicate a high quantity of metabolites and green tiles indicate a low quantity. The colored vertical bars show the molecular time of day of the metabolites. (*G* and *H*) BT measurements of mice kept under LD (*G*) and DD (*H*) conditions. Colors of the dots indicate the peak time of each molecular substance (Table S3). Peak time of the red cosine curves indicates estimated BT, and peak times of the blue indicate the environmental time. The dashed vertical lines show the BT (red) or environmental time (ZT/CT, blue). See Table S4 for statistics.

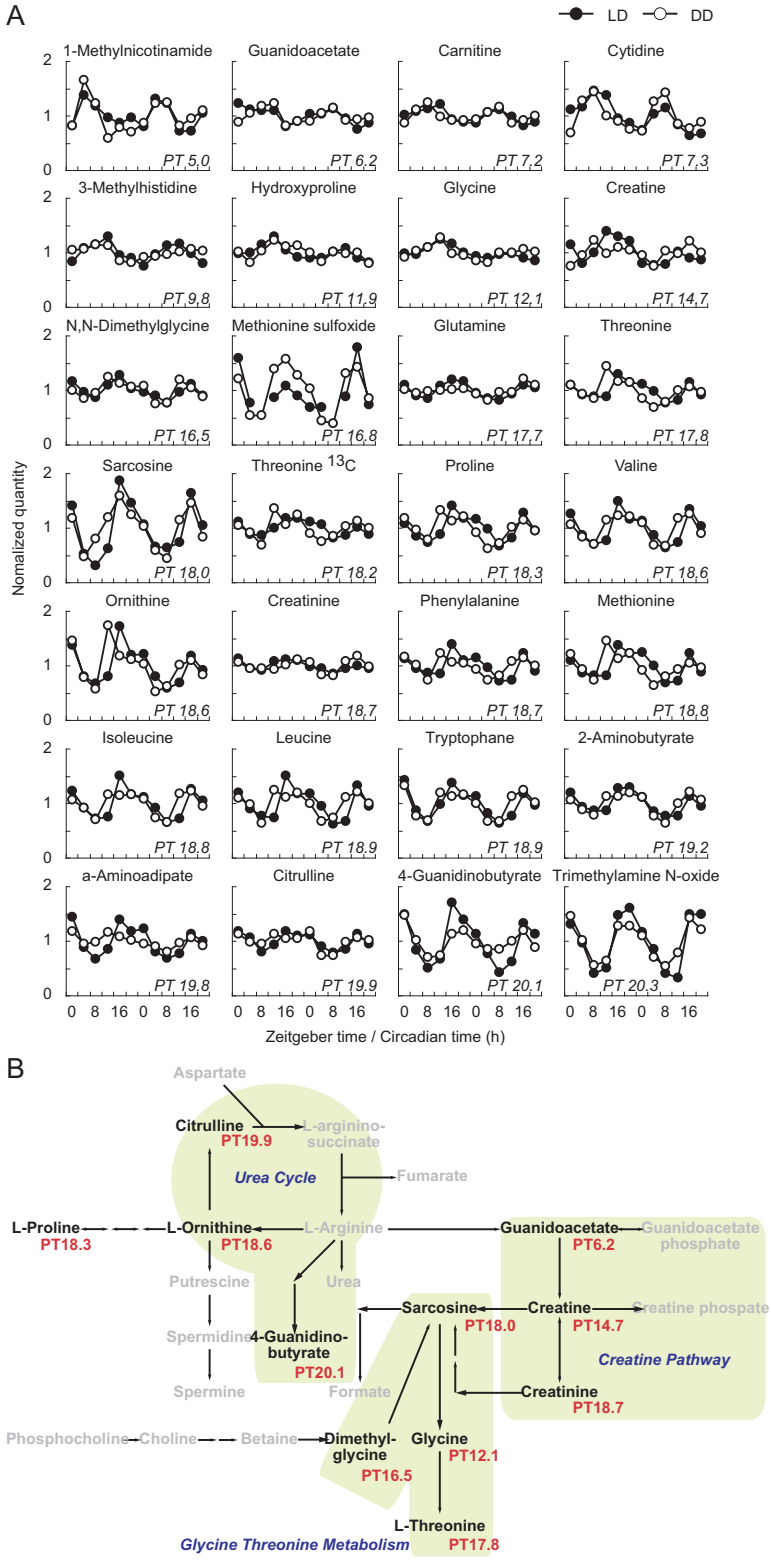

Fig. S4. Circadian rhythm of identified compounds (CE-MS). (*A*) Quantity of the substances was normalized by setting mean value as 1.0. See also Fig. S3 and Table S3. (*B*) Metabolic map. Identified circadian oscillatory metabolites are put on the known metabolic map using Ingenuity Pathway Analysis software (ver.7.0). Oscillation peak time (PT) is written in red.

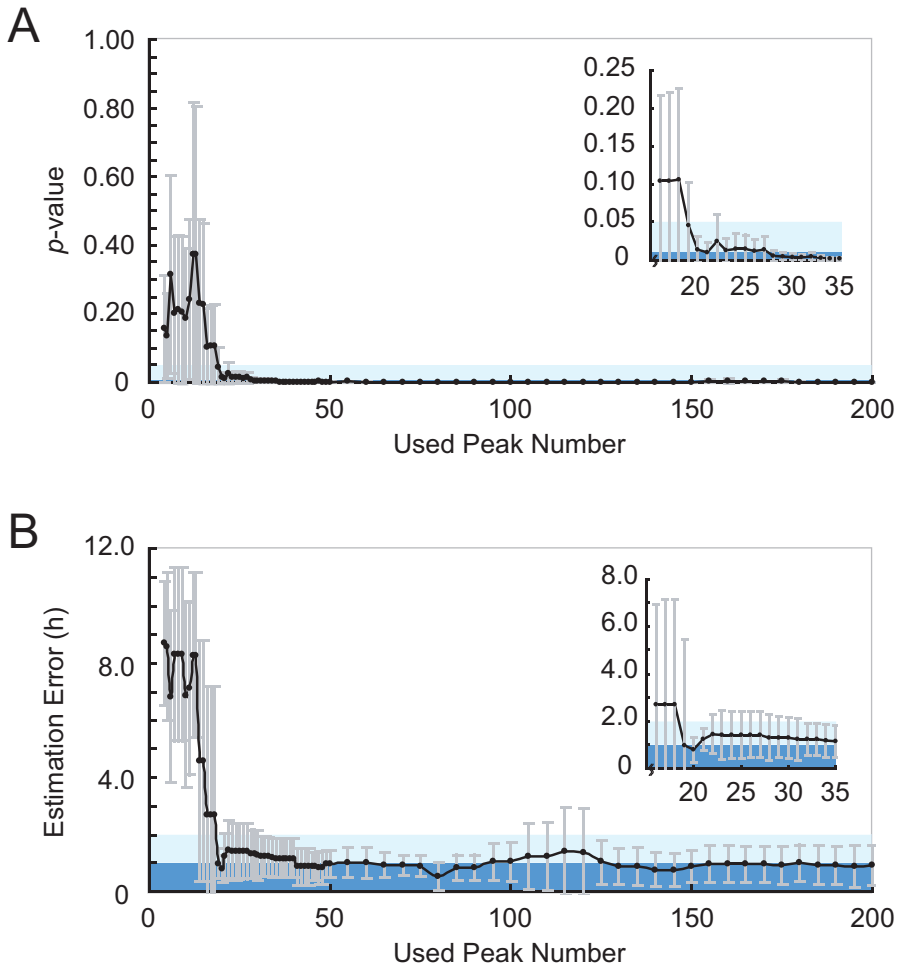

Fig. S5. Effect of the time-indicating metabolites number on the BT estimation. (*A*) Significance of the BT estimation (*P* value) changes according to the peak number used for the estimation (4–200). Magnified graph is shown as an *Inset* where used peak number change from 16–36. Light blue area indicates $P < 0.05$, and blue area indicates $P < 0.01$. (*B*) Estimation error (difference between environmental time and estimated BT) changes according to the peak number used for the estimation (4–200). Magnified graph is shown as an inset where used peak number change from 16–36. Light blue area indicates estimation error is under 2 h and blue area indicates estimation error is less than 1 h.

Table S1. Metabolite timetable for the oscillatory substances in CBA/N mice plasma analyzed by LC-MS

No.	Mode	Name	Molecular weight	Average *m/z*	Average retention time (min)	Average area	SD area	Peak time, h	Correlation	*P* value	FDR
1	positive ion			259.168	18.95	680.536	113.224	7.5	0.835	0.001	0.001
2	positive ion			263.225	15.90	1267.979	379.237	19.5	0.896	0.001	0.001
3	positive ion			277.198	15.12	1274.406	320.623	18.7	0.838	0.001	0.001
4	positive ion			277.204	14.28	296.115	119.044	18.4	0.906	0.001	0.001
5	positive ion			279.223	16.13	1554.517	419.493	18.1	0.875	0.001	0.001
6	positive ion			279.235	15.23	12662.494	4059.509	18.6	0.939	0.001	0.001
7	positive ion			280.231	15.27	930.932	427.375	18.8	0.931	0.001	0.001
8	positive ion			281.242	15.85	1846.537	642.628	19.4	0.882	0.001	0.001
9	positive ion			287.217	18.95	1786.261	169.945	9.4	0.870	0.001	0.001
10	positive ion			293.230	18.98	907.507	191.657	6.8	0.870	0.001	0.001
11	positive ion			311.237	18.95	2633.633	653.209	7.0	0.897	0.001	0.001
12	positive ion			312.236	18.95	501.591	130.407	7.0	0.885	0.001	0.001
13	positive ion			313.263	18.33	56316.017	22297.471	19.8	0.894	0.001	0.001
14	positive ion			314.278	18.38	8279.417	2963.854	19.8	0.894	0.001	0.001
15	positive ion			329.237	18.97	29876.683	12167.922	6.9	0.901	0.001	0.001
16	positive ion			330.244	18.97	5199.338	1879.800	7.0	0.902	0.001	0.001
17	positive ion			341.303	20.00	4548.040	746.126	19.2	0.843	0.001	0.001
18	positive ion			347.275	18.97	3700.810	1235.852	7.1	0.855	0.001	0.001
19	positive ion			348.218	6.97	160.043	145.686	11.1	0.844	0.001	0.001
20	positive ion			351.223	18.94	872.783	220.402	7.2	0.877	0.001	0.001
21	positive ion			353.248	18.67	293.040	97.967	19.6	0.899	0.001	0.001
22	positive ion			359.323	20.00	1109.792	287.936	19.3	0.867	0.001	0.001
23	positive ion			383.163	18.88	199.894	62.905	6.8	0.892	0.001	0.001
24	positive ion			383.332	20.18	437.545	86.679	15.3	0.867	0.001	0.001
25	positive ion			385.161	18.97	373.294	101.937	7.2	0.874	0.001	0.001
26	positive ion			387.348	20.27	774.230	337.489	19.2	0.876	0.001	0.001
27	positive ion			409.383	22.48	912.330	240.331	20.0	0.909	0.001	0.001
28	positive ion			431.319	15.82	473.819	220.486	15.2	0.923	0.001	0.001
29	positive ion			541.605	17.15	3336.822	763.362	9.1	0.863	0.001	0.001
30	positive ion			542.625	17.22	493.830	113.959	8.9	0.869	0.001	0.001
31	positive ion			543.612	18.17	1293.885	401.579	7.4	0.891	0.001	0.001
32	positive ion			544.328	19.00	5254.587	1031.599	7.6	0.871	0.001	0.001
33	positive ion	LysoPC (20:4)	543.3	544.337	17.23	564540.794	117542.644	9.1	0.870	0.001	0.001
34	positive ion			544.591	17.27	4990.002	948.585	9.0	0.862	0.001	0.001
35	positive ion			545.343	18.98	963.360	184.758	7.5	0.825	0.001	0.001
36	positive ion	LysoPC (20:3)	545.3	546.341	18.17	332357.807	101269.750	7.3	0.897	0.001	0.001
37	positive ion			546.349	17.22	15852.819	3089.025	9.3	0.886	0.001	0.001
38	positive ion			546.621	18.12	1788.982	500.325	7.2	0.902	0.001	0.001
39	positive ion			547.357	18.17	66588.046	20877.069	7.3	0.883	0.001	0.001
40	positive ion			548.348	18.20	11832.511	2896.932	7.4	0.900	0.001	0.001
41	positive ion	LysoPC (20:2)	547.4	548.365	19.28	31418.392	9477.594	6.6	0.840	0.001	0.001
42	positive ion			549.357	18.12	494.375	139.940	6.9	0.875	0.001	0.001
43	positive ion			565.491	17.25	3980.272	929.495	7.3	0.911	0.001	0.001
44	positive ion			565.571	17.33	1377.696	305.096	7.3	0.899	0.001	0.001
45	positive ion	LysoPC (22:6)	567.3	568.337	17.32	664127.323	156822.529	7.3	0.912	0.001	0.001
46	positive ion			568.622	17.30	4832.434	1126.418	7.3	0.909	0.001	0.001
47	positive ion			568.703	17.33	860.281	231.124	7.2	0.871	0.001	0.001
48	positive ion			569.346	17.30	154201.890	47981.279	7.3	0.886	0.001	0.001
49	positive ion			571.333	17.27	1201.830	291.043	7.4	0.874	0.001	0.001
50	positive ion			571.369	17.78	10150.764	2608.503	6.6	0.831	0.001	0.001
51	positive ion			279.216	14.42	731.443	173.653	18.6	0.841	0.001	0.001
52	positive ion			307.257	19.53	1538.606	262.321	7.4	0.827	0.001	0.001
53	positive ion			331.259	19.40	4657.461	995.189	6.3	0.838	0.001	0.001
54	positive ion			331.279	18.68	10034.038	3719.162	19.8	0.902	0.001	0.001
55	positive ion			332.276	18.67	1950.226	684.491	19.4	0.864	0.001	0.001
56	positive ion			347.219	6.97	1074.169	912.100	11.1	0.853	0.001	0.001
57	positive ion	LysoPC (18:1)	521.3	522.335	18.40	1438967.258	148636.948	6.7	0.853	0.001	0.001
58	positive ion			541.692	17.25	661.837	171.433	8.9	0.837	0.001	0.001
59	positive ion			545.334	17.20	122253.699	33901.935	9.3	0.863	0.001	0.001
60	positive ion			545.588	17.18	835.571	168.267	8.4	0.833	0.001	0.001
61	positive ion			636.570	25.33	169.170	136.470	20.8	0.863	0.001	0.001
62	positive ion			279.223	13.45	1160.550	350.077	18.5	0.824	0.001	0.001

No.	Mode	Name	Molecular weight	Average *m/z*	Average retention time (min)	Average area	SD area	Peak time, h	Correlation	*P* value	FDR
63	positive ion			346.270	18.97	18974.418	7461.593	7.1	0.840	0.001	0.001
64	positive ion	LysoPC (18:3)	517.3	518.327	19.00	1324.008	171.641	5.9	0.814	0.001	0.001
65	positive ion			549.375	19.28	5059.172	1504.341	6.5	0.828	0.001	0.001
66	positive ion	LysoPC (22:5)	569.3	570.348	17.77	51799.410	14327.626	6.8	0.836	0.001	0.001
67	positive ion			519.838	18.44	778.986	117.274	6.1	0.781	0.001	0.001
68	positive ion			342.300	19.95	855.019	152.425	19.3	0.796	0.001	0.001
69	positive ion			346.333	20.80	313.262	175.233	16.1	0.800	0.001	0.001
70	positive ion			318.303	19.60	371.646	212.735	16.3	0.809	0.001	0.001
71	positive ion			345.329	20.79	1571.960	841.011	16.3	0.796	0.001	0.001
72	positive ion			399.310	18.12	255.979	84.625	8.1	0.778	0.001	0.001
73	positive ion			512.331	12.72	257.272	64.113	6.2	0.793	0.001	0.001
74	positive ion			370.293	16.72	1500.262	199.518	7.5	0.781	0.001	0.001
75	positive ion			573.358	19.00	331.059	93.355	5.8	0.780	0.001	0.001
76	positive ion			550.385	19.50	3329.852	674.277	7.0	0.776	0.001	0.001
77	positive ion			566.311	16.73	1080.929	301.946	6.7	0.763	0.001	0.001
78	positive ion	LysoPC (22:4)	571.4	572.363	19.03	2313.460	607.212	5.8	0.765	0.001	0.001
79	positive ion			374.298	19.88	713.472	181.403	5.2	0.772	0.001	0.002
80	positive ion			525.371	18.40	2846.923	430.773	6.3	0.757	0.001	0.002
81	positive ion			524.358	18.40	43729.790	7838.563	6.4	0.754	0.001	0.002
82	positive ion			572.372	18.30	380.865	106.527	5.9	0.779	0.001	0.002
83	positive ion			317.301	19.60	2317.049	1147.910	16.2	0.779	0.001	0.002
84	positive ion			523.346	18.42	404594.680	75774.231	6.0	0.761	0.001	0.002
85	positive ion			548.313	17.28	1268.283	149.821	21.4	0.749	0.001	0.002
86	positive ion			523.621	18.42	2580.838	459.821	6.2	0.764	0.001	0.002
87	positive ion			521.728	18.40	610.377	140.297	5.8	0.741	0.001	0.002
88	positive ion			596.390	18.83	91.306	29.262	6.1	0.744	0.001	0.002
89	positive ion			362.355	20.78	43.167	37.661	16.5	0.775	0.001	0.002
90	positive ion			326.300	18.43	690.967	136.709	6.9	0.762	0.001	0.002
91	positive ion			520.821	18.42	872.018	181.300	5.8	0.742	0.001	0.002
92	positive ion			315.262	18.37	2923.306	306.647	18.8	0.743	0.001	0.002
93	positive ion			522.601	18.43	12091.786	2449.671	6.1	0.745	0.001	0.002
94	positive ion			373.320	19.73	98.495	62.405	19.0	0.742	0.001	0.002
95	positive ion			329.271	17.57	5496.755	1519.695	20.4	0.734	0.001	0.003
96	positive ion			504.340	18.42	3842.014	808.028	5.9	0.750	0.001	0.003
97	positive ion			436.367	17.08	485.329	157.744	10.7	0.749	0.001	0.003
98	positive ion			521.497	17.40	41.582	7.371	9.7	0.730	0.001	0.003
99	positive ion			519.727	18.43	9878.390	1981.348	6.1	0.736	0.001	0.003
100	positive ion	LysoPC (22:5)	569.3	570.366	18.30	4114.696	1380.699	6.0	0.743	0.001	0.003
101	positive ion			330.264	17.53	529.255	192.289	21.0	0.715	0.001	0.003
102	positive ion			522.841	18.35	1113.863	165.509	6.2	0.739	0.001	0.003
103	positive ion			375.335	19.08	2394.065	485.565	21.9	0.732	0.001	0.004
104	positive ion			306.240	18.98	1392.327	161.405	10.8	0.720	0.001	0.004
105	positive ion			332.344	20.70	46.496	37.272	16.5	0.715	0.001	0.004
106	positive ion			386.346	21.28	586.777	169.221	19.5	0.727	0.001	0.004
107	positive ion			520.718	18.47	3383.655	667.715	5.9	0.720	0.001	0.004
108	positive ion			345.204	12.45	78.870	46.583	18.3	0.732	0.001	0.005
109	positive ion			348.288	19.38	2629.987	618.067	6.3	0.698	0.001	0.005
110	positive ion			388.344	20.48	747.417	89.691	17.7	0.734	0.001	0.005
111	positive ion			380.272	18.98	1664.930	358.957	22.1	0.716	0.001	0.005
112	positive ion			523.132	18.45	136.258	21.291	5.8	0.713	0.001	0.005
113	positive ion			567.337	16.67	108.495	39.102	5.8	0.706	0.001	0.005
114	positive ion			549.296	17.22	150.371	27.316	22.6	0.704	0.001	0.005
115	positive ion			305.238	18.98	7870.504	959.429	10.7	0.693	0.001	0.005
116	positive ion			312.256	17.20	1031.381	252.830	20.6	0.685	0.001	0.005
117	positive ion			369.342	20.25	1971.864	301.209	17.3	0.714	0.001	0.005
118	positive ion			337.596	18.75	1763.148	346.256	22.6	0.700	0.001	0.006
119	positive ion			523.355	17.90	26718.383	3737.029	6.4	0.692	0.001	0.006
120	positive ion	LysoPC (20:3)	545.3	546.349	19.82	3780.333	402.569	7.4	0.705	0.001	0.006
121	positive ion			358.294	18.73	42123.449	9163.205	22.2	0.706	0.001	0.006
122	positive ion			505.342	18.39	707.255	184.249	5.9	0.699	0.001	0.006
123	positive ion			289.214	9.25	882.358	418.390	7.9	0.689	0.002	0.007
124	positive ion			374.327	19.07	11115.887	2772.848	21.8	0.708	0.002	0.007
125	positive ion			406.288	18.38	765.302	250.759	19.7	0.696	0.002	0.007

No.	Mode	Name	Molecular weight	Average *m/z*	Average retention time (min)	Average area	SD area	Peak time, h	Correlation	*P* value	FDR
126	positive ion			379.279	18.98	8480.791	1943.681	21.9	0.697	0.002	0.007
127	positive ion			357.281	18.73	259998.715	44246.206	22.3	0.694	0.002	0.007
128	positive ion			311.720	18.37	82.902	43.108	19.9	0.696	0.002	0.007
129	positive ion			265.247	18.75	167133.709	32570.621	22.7	0.684	0.002	0.008
130	positive ion			340.286	18.72	41660.235	9385.544	22.5	0.684	0.002	0.008
131	positive ion			327.614	18.95	87.191	45.874	7.2	0.662	0.002	0.008
132	positive ion			359.302	18.73	4316.612	718.731	22.3	0.691	0.002	0.008
133	positive ion			355.505	18.80	1833.678	334.469	22.2	0.696	0.002	0.008
134	positive ion			407.308	19.10	348.211	98.810	17.1	0.695	0.002	0.008
135	positive ion			534.349	18.32	500.526	81.959	5.7	0.691	0.002	0.008
136	positive ion			356.679	18.79	399.614	82.757	22.3	0.681	0.002	0.009
137	positive ion			337.672	19.04	69.349	19.694	21.9	0.683	0.002	0.009
138	positive ion			266.249	18.75	21598.850	4236.871	22.7	0.679	0.002	0.009
139	positive ion			324.286	17.52	102.696	26.308	6.5	0.671	0.002	0.009
140	positive ion			547.357	17.18	559.306	75.888	9.1	0.676	0.002	0.009
141	positive ion			383.310	17.08	1062.482	197.625	9.9	0.679	0.002	0.010
142	positive ion			339.278	18.75	247653.315	41743.139	22.6	0.677	0.002	0.010
1	negative ion			260.234	19.07	699.25	83.33	13.1	0.840	0.001	0.001
2	negative ion			267.147	13.60	2669.96	853.77	18.3	0.845	0.001	0.001
3	negative ion			271.230	15.68	2386.35	887.29	20.6	0.927	0.001	0.001
4	negative ion			275.194	17.45	10029.21	3439.39	21.4	0.912	0.001	0.001
5	negative ion			276.190	17.45	1285.10	380.62	21.4	0.927	0.001	0.001
6	negative ion			277.206	15.38	143.57	69.28	18.9	0.937	0.001	0.001
7	negative ion			281.817	19.00	502.83	187.97	7.0	0.906	0.001	0.001
8	negative ion			283.008	19.05	293.65	120.31	6.3	0.908	0.001	0.001
9	negative ion			283.235	19.02	133511.77	48621.92	6.8	0.917	0.001	0.001
10	negative ion			284.238	19.00	16561.78	7149.41	6.9	0.912	0.001	0.001
11	negative ion			285.250	19.45	3763.22	817.45	6.4	0.866	0.001	0.001
12	negative ion			293.211	14.43	1159.44	668.10	18.6	0.930	0.001	0.001
13	negative ion			294.206	15.22	165.46	133.80	19.1	0.830	0.001	0.001
14	negative ion			295.216	14.62	3448.61	1535.27	18.7	0.944	0.001	0.001
15	negative ion			295.216	15.38	36527.53	22337.94	18.8	0.939	0.001	0.001
16	negative ion			295.229	16.23	6106.95	2106.64	18.2	0.942	0.001	0.001
17	negative ion			296.215	16.25	311.73	130.02	18.4	0.935	0.001	0.001
18	negative ion			296.222	15.38	2900.38	1770.55	18.8	0.939	0.001	0.001
19	negative ion			297.235	15.98	29591.81	16260.51	19.3	0.939	0.001	0.001
20	negative ion			297.274	20.55	2391.15	899.28	19.6	0.914	0.001	0.001
21	negative ion			297.313	16.25	83.66	42.52	17.7	0.910	0.001	0.001
22	negative ion			298.237	15.98	3450.60	1746.22	19.4	0.942	0.001	0.001
23	negative ion			298.276	20.53	295.59	126.15	19.3	0.915	0.001	0.001
24	negative ion			299.203	17.28	3694.94	704.30	18.9	0.827	0.001	0.001
25	negative ion			306.245	19.60	31485.10	7388.69	6.9	0.844	0.001	0.001
26	negative ion			307.249	19.58	1999.29	350.71	7.4	0.856	0.001	0.001
27	negative ion			307.314	19.62	100.40	24.36	7.9	0.840	0.001	0.001
28	negative ion			315.242	14.90	936.01	234.14	18.3	0.891	0.001	0.001
29	negative ion			325.207	18.35	1568.84	409.90	7.1	0.874	0.001	0.001
30	negative ion			325.572	19.00	8503.90	3037.11	6.8	0.911	0.001	0.001
31	negative ion			326.310	19.03	201.64	76.84	6.4	0.857	0.001	0.001
32	negative ion			326.574	19.05	2122.13	725.19	6.9	0.911	0.001	0.001
33	negative ion			326.980	19.05	1267.07	229.07	6.9	0.860	0.001	0.001
34	negative ion			327.408	19.00	1027.03	344.24	6.9	0.900	0.001	0.001
35	negative ion			327.591	19.47	2330.40	535.48	6.2	0.889	0.001	0.001
36	negative ion			327.597	19.03	166.83	45.22	7.6	0.874	0.001	0.001
37	negative ion			327.984	19.05	578.33	162.43	6.3	0.898	0.001	0.001
38	negative ion			328.229	19.02	236518.78	59862.66	6.9	0.907	0.001	0.001
39	negative ion			329.241	19.47	289447.74	45967.23	6.2	0.861	0.001	0.001
40	negative ion			330.241	19.47	58655.23	14721.00	5.6	0.867	0.001	0.001
41	negative ion			331.250	19.48	3126.47	631.48	5.7	0.865	0.001	0.001
42	negative ion			348.186	15.93	361.77	237.27	18.2	0.848	0.001	0.001
43	negative ion			355.249	20.02	41345.65	12993.37	4.5	0.867	0.001	0.001
44	negative ion			356.253	19.98	6255.08	1800.34	4.7	0.868	0.001	0.001
45	negative ion			358.364	20.50	38.06	17.10	7.8	0.811	0.001	0.001
46	negative ion			373.280	20.77	306.34	277.82	19.5	0.844	0.001	0.001

No.	Mode	Name	Molecular weight	Average *m/z*	Average retention time (min)	Average area	SD area	Peak time, h	Correlation	*P* value	FDR
47	negative ion			390.259	18.45	1374.93	594.86	19.8	0.881	0.001	0.001
48	negative ion			399.306	20.93	116.58	50.29	19.1	0.848	0.001	0.001
49	negative ion			405.222	7.13	451.22	406.10	11.0	0.868	0.001	0.001
50	negative ion			417.306	19.78	1023.18	323.36	19.4	0.866	0.001	0.001
51	negative ion			427.155	19.03	493.43	228.78	6.7	0.895	0.001	0.001
52	negative ion			429.280	15.93	234.74	125.35	15.1	0.911	0.001	0.001
53	negative ion			434.224	16.82	79.23	53.78	8.2	0.885	0.001	0.001
54	negative ion			445.337	20.33	784.41	425.99	19.3	0.894	0.001	0.001
55	negative ion			446.334	20.33	113.40	68.16	19.5	0.862	0.001	0.001
56	negative ion			583.550	18.47	186.33	74.60	21.4	0.827	0.001	0.001
57	negative ion			602.321	17.33	287033.84	83159.82	9.5	0.844	0.001	0.001
58	negative ion			603.333	17.33	49999.32	15101.53	9.6	0.839	0.001	0.001
59	negative ion	LysoPC (20:3)	545.3	604.346	18.20	137734.94	49610.59	7.6	0.870	0.001	0.001
60	negative ion			604.346	19.23	635.11	159.03	7.9	0.842	0.001	0.001
61	negative ion			605.350	18.33	21222.13	7271.49	7.6	0.865	0.001	0.001
62	negative ion			605.424	17.75	314.83	95.97	8.0	0.841	0.001	0.001
63	negative ion			606.347	18.22	2143.26	603.14	7.8	0.876	0.001	0.001
64	negative ion			612.248	17.12	403.05	98.53	7.8	0.885	0.001	0.001
65	negative ion			626.021	17.42	95.75	38.00	6.8	0.918	0.001	0.001
66	negative ion			626.321	17.40	326957.21	101522.97	7.4	0.881	0.001	0.001
67	negative ion			627.335	17.43	61238.59	19734.41	7.5	0.871	0.001	0.001
68	negative ion			628.321	17.45	13762.39	3573.40	7.4	0.865	0.001	0.001
69	negative ion			635.632	19.12	644.48	176.73	22.2	0.782	0.001	0.001
70	negative ion			655.465	19.02	5139.31	3105.62	6.7	0.901	0.001	0.001
71	negative ion			656.444	19.02	1645.21	976.33	6.7	0.899	0.001	0.001
72	negative ion			659.511	18.90	264.50	92.52	24.0	0.799	0.001	0.001
73	negative ion			677.397	19.02	893.53	384.04	6.8	0.889	0.001	0.001
74	negative ion			267.233	13.57	164.97	38.82	18.1	0.832	0.001	0.001
75	negative ion			272.218	15.68	118.76	54.08	20.5	0.825	0.001	0.001
76	negative ion			275.816	18.27	2503.32	345.64	21.0	0.829	0.001	0.001
77	negative ion			278.099	15.95	271.48	166.82	18.3	0.830	0.001	0.001
78	negative ion			278.212	18.27	56882.76	10257.30	21.2	0.828	0.001	0.001
79	negative ion			293.211	15.20	1697.04	1124.21	18.9	0.856	0.001	0.001
80	negative ion			305.242	19.58	207410.93	31541.48	7.3	0.868	0.001	0.001
81	negative ion			313.236	13.58	2123.89	1348.49	18.6	0.881	0.001	0.001
82	negative ion			314.232	13.58	266.29	187.39	18.7	0.873	0.001	0.001
83	negative ion			327.224	19.03	450731.35	56454.25	8.1	0.834	0.001	0.001
84	negative ion			327.238	19.12	29224.63	11473.24	6.3	0.877	0.001	0.001
85	negative ion			327.672	19.50	263.13	59.28	6.2	0.874	0.001	0.001
86	negative ion			329.003	19.48	585.72	110.62	5.5	0.793	0.001	0.001
87	negative ion			357.272	20.50	7658.06	2367.19	7.4	0.827	0.001	0.001
88	negative ion			358.272	20.50	1321.78	385.95	7.6	0.844	0.001	0.001
89	negative ion			389.275	18.45	8513.42	3935.55	19.9	0.869	0.001	0.001
90	negative ion			455.294	15.70	69.88	44.64	18.1	0.812	0.001	0.001
91	negative ion			501.419	18.43	193.03	81.45	19.7	0.844	0.001	0.001
92	negative ion			529.296	17.27	1756.45	444.73	9.6	0.852	0.001	0.001
93	negative ion			584.446	18.47	505.60	177.06	20.9	0.845	0.001	0.001
94	negative ion			607.464	19.03	1514.24	304.87	7.2	0.842	0.001	0.001
95	negative ion			631.443	19.03	1281.79	300.32	7.7	0.851	0.001	0.001
96	negative ion			636.615	19.12	259.73	72.53	21.8	0.799	0.001	0.001
97	negative ion			303.718	19.60	1293.35	253.29	7.1	0.866	0.001	0.001
98	negative ion			328.589	19.47	326.73	70.61	5.2	0.824	0.001	0.001
99	negative ion			365.243	18.47	202.59	62.96	19.5	0.845	0.001	0.001
100	negative ion			528.279	17.28	14283.07	3410.55	9.5	0.846	0.001	0.001
101	negative ion	LysoPC (20:4)	543.3	602.017	17.35	188.55	65.59	8.9	0.857	0.001	0.001
102	negative ion			632.451	19.03	440.64	96.72	7.9	0.810	0.001	0.001
103	negative ion			347.180	15.95	2942.09	1784.65	18.2	0.832	0.001	0.001
104	negative ion			415.226	17.58	190.21	132.98	17.8	0.819	0.001	0.001
105	negative ion			432.204	16.68	143.58	122.04	10.2	0.814	0.001	0.001
106	negative ion			530.374	18.18	1374.27	159.46	9.3	0.786	0.001	0.001
107	negative ion			606.448	19.47	515.38	183.81	7.3	0.791	0.001	0.001
108	negative ion			636.511	19.13	4222.72	1281.80	21.7	0.798	0.001	0.001
109	negative ion			271.217	14.93	2699.61	829.03	20.4	0.822	0.001	0.001

No.	Mode	Name	Molecular weight	Average *m/z*	Average retention time (min)	Average area	SD area	Peak time, h	Correlation	*P* value	FDR
110	negative ion			361.186	16.67	2030.83	1244.24	18.0	0.814	0.001	0.001
111	negative ion			302.700	19.07	707.40	79.42	13.0	0.781	0.001	0.001
112	negative ion			590.305	18.22	315.38	112.03	7.5	0.817	0.001	0.001
113	negative ion			635.518	19.12	15619.10	5433.97	21.8	0.798	0.001	0.001
114	negative ion			285.301	19.73	213.42	52.55	5.5	0.774	0.001	0.001
115	negative ion			305.013	19.62	429.06	83.27	6.1	0.779	0.001	0.001
116	negative ion			316.221	18.87	2345.52	501.71	4.3	0.786	0.001	0.001
117	negative ion			411.242	19.47	493.95	85.87	6.3	0.802	0.001	0.001
118	negative ion			605.424	19.05	53.32	28.87	16.3	0.760	0.001	0.001
119	negative ion			637.494	19.13	635.78	168.22	21.6	0.798	0.001	0.001
120	negative ion			259.237	19.05	4932.97	591.47	12.5	0.740	0.001	0.001
121	negative ion			582.482	17.98	1665.76	144.72	5.9	0.791	0.001	0.001
122	negative ion			530.279	18.17	24088.60	2362.84	9.2	0.771	0.001	0.001
123	negative ion	LysoPC (20:2)	547.4	606.365	19.40	8001.49	2697.91	7.0	0.799	0.001	0.001
124	negative ion			315.222	18.90	15615.44	3900.23	4.1	0.777	0.001	0.001
125	negative ion			401.316	21.75	342.66	374.48	20.1	0.748	0.001	0.001
126	negative ion			445.408	20.32	38.83	26.51	19.4	0.774	0.001	0.001
127	negative ion			598.500	18.85	313.28	49.32	20.4	0.771	0.001	0.001
128	negative ion			607.344	19.37	1428.89	446.19	7.0	0.771	0.001	0.001
129	negative ion			297.235	17.30	1060.40	296.29	16.6	0.767	0.001	0.002
130	negative ion			361.222	19.15	1587.67	251.50	16.9	0.779	0.001	0.002
131	negative ion			657.443	19.05	446.64	139.95	5.5	0.763	0.001	0.002
132	negative ion	LysoPC (18:1)	521.3	580.033	18.58	1217.29	223.87	6.1	0.751	0.001	0.002
133	negative ion			399.254	20.93	911.99	350.94	19.5	0.796	0.001	0.002
134	negative ion			347.277	20.57	66.75	78.55	19.2	0.741	0.001	0.002
135	negative ion			269.246	20.00	27628.91	2755.49	13.6	0.753	0.001	0.002
136	negative ion			457.287	14.25	177.72	121.91	18.0	0.769	0.001	0.002
137	negative ion			270.249	20.00	2223.62	210.57	12.9	0.724	0.001	0.003
138	negative ion			507.412	18.52	892.79	236.54	6.0	0.739	0.001	0.003
139	negative ion			581.469	17.98	13108.88	1268.01	6.5	0.720	0.001	0.003
140	negative ion			301.703	19.05	3780.29	376.48	12.6	0.692	0.001	0.003
141	negative ion			388.263	17.33	238.19	106.88	21.0	0.709	0.001	0.003
142	negative ion			311.276	20.00	335.03	76.10	4.7	0.736	0.001	0.004
143	negative ion			387.267	17.33	2229.61	986.54	21.2	0.709	0.001	0.004
144	negative ion			302.211	18.28	51542.47	7727.26	0.3	0.723	0.001	0.004
145	negative ion			258.231	18.27	1627.47	193.54	0.5	0.721	0.001	0.004
146	negative ion			257.220	18.28	12024.18	1646.18	0.5	0.719	0.001	0.004
147	negative ion			606.420	19.47	135.94	39.69	7.0	0.732	0.001	0.004
148	negative ion			343.190	12.60	122.65	82.99	19.1	0.723	0.001	0.004
149	negative ion			302.746	19.05	190.05	23.92	12.9	0.720	0.001	0.004
150	negative ion			277.212	18.27	343760.84	25938.67	20.7	0.708	0.001	0.005
151	negative ion			387.333	17.33	115.34	53.59	21.5	0.693	0.001	0.005
152	negative ion			409.223	19.02	707.95	134.45	7.6	0.720	0.001	0.005
153	negative ion			690.432	17.28	14586.74	1345.28	19.4	0.729	0.001	0.005
154	negative ion			628.339	18.40	754.37	225.87	6.3	0.719	0.001	0.005
155	negative ion			580.349	18.57	820445.27	113697.08	7.0	0.705	0.001	0.005
156	negative ion			611.479	18.85	193.68	60.29	21.4	0.695	0.001	0.005
157	negative ion			303.216	18.28	2867.41	292.34	0.4	0.712	0.001	0.006
158	negative ion			626.321	19.22	819.30	114.82	8.0	0.696	0.001	0.006
159	negative ion			508.349	18.52	124.40	42.87	5.4	0.707	0.001	0.006
160	negative ion			303.222	19.10	404198.50	24331.25	10.5	0.702	0.001	0.006
161	negative ion			597.492	18.83	1068.86	173.61	20.8	0.694	0.002	0.007
162	negative ion			580.449	18.05	1194.48	238.56	7.0	0.687	0.002	0.007
163	negative ion			400.236	20.95	61.51	40.98	20.2	0.688	0.002	0.007
164	negative ion			280.228	14.67	1989.29	180.70	12.6	0.678	0.002	0.007
165	negative ion			329.309	19.70	707.18	150.52	5.2	0.695	0.002	0.008
166	negative ion			564.301	17.28	14590.87	1592.32	20.1	0.675	0.002	0.008
167	negative ion			580.340	18.03	37125.78	8182.82	7.0	0.673	0.002	0.008
168	negative ion			252.202	17.60	822.16	144.98	6.0	0.687	0.002	0.008
169	negative ion			631.462	18.27	1638.61	591.39	21.4	0.685	0.002	0.009
170	negative ion			303.255	19.18	2617.81	452.96	6.5	0.687	0.002	0.009
171	negative ion			375.317	21.53	1609.00	2118.80	19.8	0.644	0.002	0.009
172	negative ion			691.407	17.33	3502.35	322.87	19.1	0.688	0.002	0.009

No.	Mode	Name	Molecular weight	Average *m/z*	Average retention time (min)	Average area	SD area	Peak time, h	Correlation	*P* value	FDR
173	negative ion			416.303	18.87	27353.02	7027.05	22.4	0.679	0.002	0.009
174	negative ion			279.388	19.07	2453.37	304.13	19.8	0.667	0.002	0.010
175	negative ion			558.299	18.65	2073.03	254.35	8.0	0.662	0.002	0.010
176	negative ion			278.430	19.08	59.38	9.77	18.5	0.672	0.002	0.010

″Mode″ indicates a detection mode of the LC-MS instruction. ″Name″ and ″MW″ indicate the name of the substance and its molecular weight, if found. ″Average *m/*″′, ″Average retention time (min)″, ″Average area″, and ″SD area″ indicate a mean *m/z* value, a mean retention time, a mean area, and a standard deviation area of 24 time points (LD 12 time points + DD 12 time points) for associated peaks, respectively. The ″Peak time″, ″Correlation″, ″*P* value,″ and ″FDR″ indicate the results of the statistical analysis of the circadian oscillation and represent a peak time of circadian oscillation, the maximum Pearson's correlation to a fitted cosine curve, *P* value, and FDR estimations of its significance, respectively. *P* values and FDRs were rounded up, and the other values were rounded off. LysoPC, lysophosphatidylcholine (positive ion $[M + H^+]^+$, negative ion $[M + CH3COO^-]^-$).

Table S2. Results of the BT estimations using LC-MS

Strain	Age	Sex	LD/DD	Feeding	Condition	Peak (used/all)	ZT/CT, h	BT, h	Difference, h	Correlation	*P* value	Figure
CBA/N	Young	male	LD (ZT)	*ad lib*	entrained	93/161	0	23.5	0.5	0.664	0.001	Fig. 2, 4
						91/160	4	3.0	1.0	0.465	0.001	Fig.2
						85/152	8	6.4	1.6	0.810	0.001	Fig.2
						93/161	12	11.5	0.5	0.664	0.001	Fig.2, 4
						92/160	16	15.0	1.0	0.465	0.001	Fig.2
						83/152	20	18.4	1.6	0.810	0.001	Fig.2
CBA/N	Young	male	DD (CT)	*ad lib*	entrained	94/160	0	0.8	0.8	0.541	0.001	Fig.2
						84/158	4	2.7	1.3	0.509	0.001	Fig.2
						97/159	8	6.2	1.8	0.840	0.001	Fig.2
						94/160	12	12.8	0.8	0.541	0.001	Fig.2
						90/158	16	14.7	1.3	0.509	0.001	Fig.2
						97/159	20	18.2	1.8	0.840	0.001	Fig.2
C57Bl/6	Young	male	LD (ZT)	*ad lib*	entrained	99/160	0	22.0	2.0	0.812	0.001	Fig.3
						96/155	4	2.4	1.6	0.774	0.001	Fig.3
						94/159	8	9.2	1.2	0.867	0.001	Fig.3
						97/160	12	10.0	2.0	0.812	0.001	Fig.3
						98/155	16	14.4	1.6	0.774	0.001	Fig.3
						91/159	20	21.2	1.2	0.867	0.001	Fig.3
C57Bl/6	Young	male	DD (CT)	*ad lib*	entrained	93/153	0	22.0	2.0	0.638	0.001	Fig.3
						93/160	4	2.5	1.5	0.823	0.001	Fig.3
						100/161	8	6.4	1.6	0.884	0.001	Fig.3
						94/153	12	10.0	2.0	0.638	0.001	Fig.3
						96/160	16	14.5	1.5	0.823	0.001	Fig.3
						101/161	20	18.4	1.6	0.884	0.001	Fig.3
CBA/N	Young	male	LD (ZT)	Food deprivation	entrained	98/161	0	1.6	1.6	0.459	0.001	Fig.4
						98/161	4	1.7	2.3	0.336	0.006	Fig.4
						105/161	8	5.3	2.7	0.277	0.019	Fig.4
						99/161	12	13.6	1.6	0.459	0.001	Fig.4
						99/161	16	13.7	2.3	0.336	0.005	Fig.4
						105/161	20	17.3	2.7	0.277	0.016	Fig.4
CBA / N	Aged	male	LD (ZT)	*ad lib*	entrained	91/160	0	23.0	1.0	0.636	0.001	Fig.4
						95/160	12	11.0	1.0	0.636	0.001	Fig.4
CBA / N	Young	female	LD (ZT)	*ad lib*	entrained	100/160	0	1.2	1.2	0.734	0.001	Fig.4
						100/160	12	13.2	1.2	0.734	0.001	Fig.4
CBA / N	Young	male	LD (ZT)	*ad lib*	Jet-lagged (Day1)	89/153	0*	23.8	0.2	0.814	0.001	Fig.5
						87/153	12*	11.8	0.2	0.814	0.001	Fig.5
						89/155	0*	0.9	0.9	0.586	0.001	Fig.S2
						92/155	12*	12.9	0.9	0.586	0.001	Fig.S2
CBA / N	Young	male	LD (ZT)	*ad lib*	Jet-lagged (Day5)	87/151	0*	3.5	3.5	0.573	0.001	Fig.5
						87/151	12*	15.5	3.5	0.573	0.001	Fig.5
						84/160	0*	3.2	3.2	0.563	0.001	Fig.S2
						84/160	12*	15.2	3.2	0.563	0.001	Fig.S2
CBA / N	Young	male	LD (ZT)	*ad lib*	Jet-lagged (Day14)	94/161	0*	8.8	8.8	0.889	0.001	Fig.5
						94/161	12*	20.8	8.8	0.889	0.001	Fig.5

The ″Peak″ indicates as used peaks number (″Used″) over associated oscillatory peaks in the samples (″All″). ″ZT/CT″ indicates environmental time in ZT (LD conditions) or CT (DD conditions) when the sample was taken. The ″Difference″ is determined as follows: BT - (environmental time) . Asterisks (*) indicates the zeitgeber time in original LD cycles before mice were released into new LD cycle in jet-lag experiments. See Table S1 for used oscillatory peaks information (metabolite timetable). See also *Materials and Methods* for details. LD, light-dark; DD, constant dark; ZT, zeitgeber time; CT, circadian time.

Table S3. Metabolite timetable for the oscillatory substances in CBA/N mice plasma analyzed by CE-MS

No.	Name	Average *m/z*	Average MT	Average area/area (IS1)	SD area/area (IS1)	Peak time (h)	Correlation	*P* value	FDR
1	Trimethylamine N-oxide	76.08	8.56	0.02	0.01	20.3	0.901	0.001	0.003
2		147.38	13.41	0.00	0.00	17.8	0.819	0.001	0.003
3		161.13	9.16	0.01	0.00	20.7	0.852	0.001	0.003
4		259.09	12.85	0.00	0.00	6.8	0.890	0.001	0.003
5		61.04	24.05	3.33	0.55	19.3	0.812	0.001	0.004
6		134.11	12.80	0.00	0.00	18.7	0.802	0.001	0.004
7		381.10	24.88	0.01	0.00	7.3	0.788	0.001	0.004
8		121.07	24.05	0.17	0.05	19.3	0.804	0.001	0.004
9	Glutamine	147.08	13.41	1.08	0.12	17.7	0.804	0.001	0.004
10	2-Aminobutyrate	104.07	12.16	0.01	0.00	19.2	0.814	0.001	0.004
11		148.08	13.40	0.06	0.01	17.9	0.802	0.001	0.004
12	Cytidine	244.09	12.18	0.01	0.00	7.3	0.791	0.001	0.004
13		261.14	15.78	0.01	0.00	19.2	0.780	0.001	0.004
14	Sarcosine	90.06	11.97	0.00	0.00	18.0	0.814	0.001	0.004
15		144.10	14.29	0.04	0.01	19.5	0.798	0.001	0.004
16		147.28	13.41	0.01	0.00	17.9	0.808	0.001	0.004
17		62.04	24.05	0.06	0.01	19.4	0.793	0.001	0.004
18		143.05	24.04	0.14	0.02	19.3	0.808	0.001	0.004
19		265.06	24.02	0.01	0.00	19.9	0.803	0.001	0.005
20		84.05	13.40	0.02	0.00	17.7	0.786	0.001	0.005
21		130.05	13.40	0.07	0.01	17.8	0.773	0.001	0.005
22		83.02	24.02	0.25	0.04	19.3	0.777	0.001	0.005
23		72.08	12.58	0.13	0.03	18.5	0.779	0.001	0.005
24	Carnitine	162.11	10.84	0.18	0.02	7.2	0.773	0.001	0.005
25		132.29	12.80	0.00	0.00	20.0	0.839	0.001	0.005
26	Valine	118.09	12.58	1.27	0.31	18.6	0.775	0.001	0.005
27		168.08	10.07	0.01	0.00	21.2	0.763	0.001	0.006
28		276.12	15.87	0.01	0.00	19.1	0.772	0.001	0.006
29		86.10	12.81	0.06	0.01	19.2	0.762	0.001	0.007
30		383.12	24.89	0.14	0.01	7.2	0.758	0.001	0.007
31	Tryptophan	205.10	13.70	0.24	0.06	18.9	0.756	0.001	0.007
32		138.06	13.09	0.01	0.00	19.1	0.766	0.001	0.008
33	4-Guanidinobutyrate	146.09	10.56	0.00	0.00	20.1	0.749	0.001	0.008
34		145.05	24.93	0.21	0.01	7.6	0.755	0.001	0.009
35	Isoleucine	132.10	12.80	0.68	0.16	18.8	0.749	0.001	0.009
36		119.09	12.58	0.06	0.02	18.6	0.756	0.001	0.009
37		248.15	12.39	0.00	0.00	7.0	0.748	0.001	0.009
38		132.10	12.78	0.68	0.16	18.8	0.750	0.001	0.009
39		817.85	6.87	0.00	0.00	6.6	0.779	0.001	0.010
40		206.10	13.70	0.03	0.01	18.8	0.744	0.001	0.010
41		133.11	12.80	0.04	0.01	18.8	0.736	0.001	0.010
42		203.05	24.94	0.24	0.02	7.5	0.719	0.001	0.010
43		133.11	12.80	0.04	0.01	18.9	0.741	0.001	0.010
44		204.06	24.90	0.02	0.00	7.5	0.750	0.001	0.010
45		152.58	11.08	0.00	0.00	22.9	0.712	0.001	0.011
46		188.07	13.70	0.02	0.00	18.9	0.726	0.001	0.011
47		360.08	24.90	0.02	0.00	9.8	0.724	0.001	0.011
48		296.15	11.34	0.00	0.00	19.8	0.733	0.001	0.011
49		207.10	13.70	0.00	0.00	18.8	0.731	0.001	0.011
50	3-Methylhistidine	170.09	9.64	0.02	0.00	9.8	0.724	0.001	0.011
51		387.60	24.93	0.03	0.00	6.4	0.718	0.001	0.012
52		133.11	12.92	0.07	0.02	19.2	0.721	0.001	0.013
53		258.90	5.40	0.00	0.00	4.2	0.715	0.001	0.013
54		107.05	12.54	0.01	0.00	10.3	0.691	0.001	0.013
55		134.11	12.91	0.01	0.00	19.0	0.710	0.001	0.013
56	Leucine	132.10	12.92	1.32	0.32	18.9	0.711	0.001	0.014
57		154.08	12.81	0.01	0.00	19.0	0.712	0.001	0.014
58	Proline	116.07	13.49	0.31	0.07	18.3	0.713	0.001	0.015
59		85.03	24.93	0.14	0.01	7.3	0.720	0.001	0.015
60		162.13	9.16	0.00	0.00	19.9	0.717	0.001	0.015
61		380.11	24.93	0.05	0.01	6.0	0.715	0.001	0.015
62		140.07	12.58	0.01	0.00	18.3	0.707	0.001	0.015

No.	Name	Average *m/z*	Average MT	Average area/area (IS1)	SD area/area (IS1)	Peak time (h)	Correlation	*P* value	FDR
63		860.84	6.84	0.00	0.00	10.3	0.710	0.001	0.015
64	Guanidoacetate	118.06	10.51	0.01	0.00	6.2	0.709	0.002	0.015
65		133.11	12.92	0.07	0.02	19.1	0.699	0.002	0.015
66		915.32	6.91	0.00	0.00	5.4	0.711	0.002	0.016
67		132.10	12.92	1.29	0.31	18.8	0.699	0.002	0.016
68		290.08	24.90	0.04	0.00	6.2	0.715	0.002	0.016
69		276.16	12.15	0.00	0.00	8.3	0.689	0.002	0.016
70		295.15	11.34	0.01	0.00	19.4	0.707	0.002	0.017
71		384.12	24.93	0.02	0.00	7.8	0.689	0.002	0.017
72	1-Methylnicotinamide	137.07	9.46	0.00	0.00	5.0	0.689	0.002	0.017
73		86.10	12.92	0.10	0.02	18.8	0.696	0.002	0.018
74		160.13	10.74	0.02	0.00	8.6	0.681	0.002	0.018
75		309.17	11.15	0.02	0.00	22.5	0.686	0.002	0.018
76		70.07	13.49	0.02	0.00	18.2	0.686	0.002	0.019
77		191.14	9.74	0.01	0.00	18.4	0.698	0.002	0.019
78		252.18	12.58	0.00	0.00	18.0	0.674	0.002	0.021
79		157.08	9.41	0.02	0.00	21.1	0.677	0.002	0.023
80		242.03	24.76	0.00	0.00	16.1	0.649	0.002	0.023
81		205.12	11.65	0.00	0.00	20.1	0.665	0.003	0.027
82	Citrulline	176.10	13.75	0.14	0.02	19.9	0.668	0.003	0.027
83		61.15	24.02	0.20	0.11	19.1	0.715	0.003	0.027
84		218.14	11.78	0.00	0.00	14.8	0.664	0.003	0.028
85		247.13	15.55	0.00	0.00	17.9	0.675	0.003	0.028
86		939.83	6.82	0.00	0.00	7.4	0.694	0.003	0.029
87	Creatinine	114.07	9.40	0.01	0.00	18.7	0.659	0.003	0.029
88		295.13	15.91	0.00	0.00	18.9	0.680	0.003	0.029
89		145.11	14.29	0.00	0.00	19.3	0.661	0.003	0.031
90		69.04	24.89	0.03	0.00	7.0	0.657	0.004	0.032
91		276.22	12.95	0.17	0.01	7.4	0.649	0.004	0.035
92		106.95	5.40	0.02	0.00	3.9	0.649	0.004	0.035
93		266.20	12.92	0.01	0.00	18.5	0.654	0.004	0.035
94		117.07	13.49	0.02	0.00	18.0	0.652	0.004	0.035
95		477.16	13.40	0.00	0.00	18.4	0.686	0.004	0.035
96		352.58	24.86	0.03	0.00	8.3	0.650	0.004	0.037
97		159.04	5.40	0.02	0.00	8.1	0.647	0.004	0.039
98		475.07	24.81	0.01	0.00	14.5	0.635	0.005	0.041
99	Glycine	76.04	10.61	0.19	0.02	12.1	0.623	0.005	0.043
100		340.87	5.40	0.00	0.00	6.0	0.659	0.005	0.043
101		263.15	11.22	0.01	0.00	14.9	0.635	0.005	0.046
102		149.08	13.39	0.01	0.00	17.4	0.616	0.006	0.047
103		380.60	24.90	0.02	0.00	6.6	0.635	0.006	0.049
104		132.39	12.92	0.01	0.00	19.2	0.634	0.006	0.050
105		159.08	13.75	0.01	0.00	20.5	0.630	0.006	0.050
106		514.88	6.82	0.00	0.00	6.3	0.621	0.006	0.050
107		177.11	13.75	0.01	0.00	20.1	0.622	0.006	0.050
108		317.10	13.40	0.00	0.00	17.7	0.624	0.006	0.050
109	Methionine sulfoxide	166.05	14.64	0.01	0.00	16.8	0.655	0.006	0.051
110		95.06	24.91	0.04	0.00	11.3	0.618	0.006	0.052
111	a-Aminoadipate	162.08	13.65	0.00	0.00	19.8	0.621	0.007	0.056
112		154.08	12.92	0.01	0.00	19.1	0.624	0.007	0.056
113		416.20	11.24	0.00	0.00	15.1	0.616	0.007	0.057
114		277.22	12.81	0.01	0.00	7.3	0.640	0.007	0.058
115		192.91	5.41	0.00	0.00	3.7	0.613	0.007	0.058
116		297.57	24.99	0.03	0.00	7.4	0.636	0.008	0.059
117		90.06	11.22	0.01	0.00	14.9	0.619	0.008	0.059
118	Methionine	150.06	13.37	0.21	0.05	18.8	0.620	0.008	0.059
119		398.11	24.91	0.03	0.00	8.0	0.603	0.008	0.059
120		121.57	8.86	0.00	0.00	16.5	0.619	0.008	0.059
121		245.09	24.83	0.02	0.00	8.3	0.612	0.008	0.059
122		995.48	6.83	0.00	0.00	23.7	0.665	0.008	0.061
123		91.04	25.51	0.02	0.00	18.7	0.627	0.008	0.061
124	Phenylalanine	166.09	13.79	0.40	0.07	18.7	0.614	0.008	0.061
125	N,N-Dimethylglycine	104.07	13.63	0.01	0.00	16.5	0.617	0.008	0.061

No.	Name	Average *m/z*	Average MT	Average area/area (IS1)	SD area/area (IS1)	Peak time (h)	Correlation	*P* value	FDR
126		908.83	6.89	0.00	0.00	18.8	0.619	0.009	0.062
127		152.06	13.37	0.01	0.00	19.3	0.616	0.009	0.063
128		121.07	8.94	0.01	0.00	15.9	0.609	0.009	0.063
129		70.07	8.83	0.01	0.00	18.4	0.603	0.010	0.067
130		852.84	6.89	0.00	0.00	13.6	0.603	0.010	0.067
131		116.07	8.83	0.02	0.01	18.6	0.600	0.010	0.067
132		110.07	9.40	0.01	0.00	20.4	0.603	0.010	0.072
133		295.06	25.51	0.06	0.01	19.8	0.600	0.011	0.073
134	Thr ^{13}C	121.07	13.14	0.01	0.00	18.2	0.597	0.011	0.074
135		225.04	25.51	0.01	0.00	18.8	0.597	0.011	0.074
136		134.10	8.83	0.01	0.00	18.5	0.594	0.011	0.074
137		151.06	13.37	0.01	0.00	19.2	0.601	0.011	0.075
138		276.87	5.41	0.00	0.00	4.0	0.589	0.011	0.075
139		325.11	24.93	0.07	0.01	7.5	0.615	0.011	0.075
140	Threonine	120.07	13.14	0.33	0.06	17.8	0.592	0.012	0.075
141	Ornithine	133.10	8.83	0.24	0.08	18.6	0.594	0.012	0.075
142		396.83	5.39	0.00	0.00	3.8	0.601	0.012	0.075
143		167.09	13.79	0.03	0.01	18.8	0.593	0.012	0.075
144		385.09	24.95	0.17	0.02	7.1	0.600	0.012	0.076
145		190.91	5.39	0.01	0.00	3.6	0.586	0.012	0.078
146		277.22	12.95	0.02	0.00	8.4	0.585	0.013	0.081
147		131.57	10.82	0.00	0.00	19.1	0.621	0.013	0.081
148		262.55	24.88	0.02	0.00	9.2	0.583	0.014	0.086
149		138.58	10.93	0.00	0.00	0.2	0.577	0.014	0.088
150		200.55	25.29	0.00	0.00	5.8	0.590	0.014	0.089
151	Hydroxyproline	132.07	14.85	0.03	0.00	11.9	0.577	0.015	0.092
152		108.95	5.41	0.00	0.00	4.5	0.581	0.015	0.093
153	Creatine	132.08	11.21	1.35	0.25	14.7	0.578	0.016	0.097

The ″Name″ column indicate the name of the substance if found. The ″Average *m/z*″, ″Average MT″, ″Average area/area (IS1)″, ″SD area/area (IS1)″ columns indicate a mean *m/z* value, a mean retention time, a mean area and a standard deviation area divided by the area of an internal standard (methionine sulfone) of 24 time points (LD 12 time points + DD 12 time points) for each associated peaks, respectively. ″Peak time″, ″Correlation″, ″*P* value″ and ″FDR″ indicate the results of the statistical analysis of the circadian oscillation and represent a peak time of circadian oscillation, the maximum Pearson's correlation to a fitted cosine curve, *P* value and FDR estimations of its significance, respectively. *P* values and FDRs were rounded up and the other values were rounded off. All 153 peaks information was used to estimate BT (FDR < 0.1, Fig. S3 *A–D*). For BT estimation using much severer condition (FDR < 0.01), 44 peaks information (no.1- 4) was used (Fig. S3 *E–H*).

Table S4. Results of the BT estimations using CE-MS

Strain	Age	Sex	LD/DD	Feeding	Condition	Peak (used/all)	ZT/CT (h)	BT (h)	Difference (h)	Correlation	*P* value	Figure
CBA/N	Young	Male	LD	ad lib	entrained	100/129	0	0.7	0.7	0.519	0.001	Fig. S3
(FDR < 0.1)			(ZT)			97/127	4	4.2	0.2	0.638	0.001	Fig. S3
						97/127	8	7.2	0.8	0.830	0.001	Fig. S3
						100/129	12	12.7	0.7	0.519	0.001	Fig. S3
						97/127	16	16.2	0.2	0.638	0.001	Fig. S3
						97/127	20	19.2	0.8	0.830	0.001	Fig. S3
CBA/N	Young	Male	DD	ad lib	entrained	98/132	0	23.7	0.3	0.523	0.001	Fig. S3
(FDR < 0.1)			(CT)			99/129	4	3.8	0.2	0.738	0.001	Fig. S3
						99/129	8	6.7	1.3	0.755	0.001	Fig. S3
						98/132	12	11.7	0.3	0.523	0.001	Fig. S3
						99/129	16	15.8	0.2	0.738	0.001	Fig. S3
						99/129	20	18.7	1.3	0.755	0.001	Fig. S3
CBA/N	Young	Male	LD	ad lib	entrained	31/39	0	0.5	0.5	0.598	0.002	Fig. S3
(FDR < 0.01)			(ZT)			30/39	4	1.9	2.1	0.872	0.001	Fig. S3
						31/38	8	6.2	1.8	0.878	0.001	Fig. S3
						31/39	12	12.5	0.5	0.598	0.003	Fig. S3
						30/39	16	13.9	2.1	0.872	0.001	Fig. S3
						31/38	20	18.2	1.8	0.878	0.001	Fig. S3
CBA/N	Young	Male	DD	ad lib	entrained	31/41	0	0.5	0.5	0.605	0.003	Fig. S3
(FDR < 0.01)			(CT)			32/41	4	2.7	1.3	0.729	0.001	Fig. S3
						29/39	8	5.5	2.5	0.897	0.001	Fig. S3
						31/41	12	12.5	0.5	0.605	0.003	Fig. S3
						32/41	16	14.7	1.3	0.729	0.001	Fig. S3
						29/39	20	17.5	2.5	0.897	0.001	Fig. S3

The ″Peak″ indicates as used peaks number (″Used″) over associated oscillatory peaks in the samples (″All″). ″ZT/CT″ indicates environmental time in ZT (LD conditions) or CT (DD conditions) when the sample was taken. The ″Difference″ is determined as follows: BT - (environmental time). See Table S3 for used oscillatory peaks information (metabolite timetable). See also *Materials and Methods* for details. LD; light-dark, DD; constant dark, ZT; zeitgeber time, CT; circadian time.